Eur Biophys J (1999) 28: 393–414

ARTICLE

Alexander Syganow · Eberhard von Kitzing

The drift approximation solves the Poisson, Nernst-Planck, and continuum equations in the limit of large external voltages

Received: 24 September 1998 / Revised version: 22 January 1999 / Accepted: 22 January 1999

Abstract Nearly linear current-voltage curves are frequently found in biological ion channels. Using the drift limit of the substantially non-linear Poisson-Nernst-Planck equations, we explain such behavior of diffusion-controlled charge transport systems. Starting from Gauss' law, drift, and continuity equations we derive a simple analytical current-voltage relation, which accounts for this deviation from linearity. As shown previously, the drift limit of the Nernst-Planck equation applies if the total electric current is dominated by the electric field, and integral contributions from concentration gradients are small. The simple analytical form of the drift current-voltage relations makes it an ideal tool to analyze experiment current-voltage curves. We also solved the complete Poisson-Nernst-Planck equations numerically, and determined current-voltage curves over a wide range of voltages, concentrations, and Debye lengths. The simulation fully supports the analytical estimate that the current-voltage curves of simple charge transport systems are dominated by the drift mechanism. Even those relations containing the most extensive approximations remained qualitatively within the correct order of magnitude.

Key words Nernst-Planck equation · Gauss' law · Poisson equation · Continuity equation · Drift charge transport mechanism

Introduction

The Nernst-Planck equation (Sze 1981; Hoppe et al. 1982; Buck 1984; Cooper et al. 1985; Rubinstein 1990; Hille 1992) is often used as a starting point to describe diffusion-controlled ion transport. Permanent charges form the channel walls, and mobile ions generate an electric field that superimposes on the electric field created by the external voltage V. Consequently, Gauss' law or the equivalent Poisson equation (Jackson 1962) must also be satisfied. Implicitly, the conservation of the number of permanent ions is generally assumed. If pairing occurs, association and dissociation of oppositely charged ions, a pairing term has to be taken into account (Lampert and Mark 1970; Buck 1984). The Poisson or Gauss, Nernst-Planck, and continuity equations (PNPC) represent a general framework to explain ion transport through biological ion channels. Despite the complexity of the PNPC equations, many experimental diffusion-controlled charge transport systems display rather simple, close to linear current-voltage curves.

The drift current-voltage relations presented in this article are rather general; they apply to biological ion channels and ion exchange membranes as well as to semiconductors. Table 1 compares the terminologies introduced into the different fields where the PNPC theory is used to describe diffusion-controlled charge transport. This table is an extension to the one given by Rubinstein (1990) to translate between semiconductors and ion exchange membranes. The terminology and examples used in this article are taken from the field of biological ion channels.

The PNPC equations represent a set of coupled, nonlinear differential equations for which a general analytic solution is not available. Particular solutions exist, however, for certain limiting situations, e.g., for *short* or *long* systems. In a short system the screening length l, e.g., the Debye length l_{DH}, is large compared to the system length ($L \ll l$). A well-studied short system theory was proposed by Goldman, Hodgkin and Katz (GHK theory) (Goldman 1943; Hodgkin and Katz 1949; MacGillivray and Hare 1969; Cooper et al. 1985; Hille 1992) to describe ion permeation through biological ion channels. The central characteristic of short systems is that the charge carriers do not interact with each other, because they leave the channel before such an interaction can occur. In long systems with $L > l$ the behavior of mobile charge carriers is determined by strong mutual interactions. Except for a boundary layer

A. Syganow · E. von Kitzing (✉)
Abteilung Zellphysiologie,
Max-Planck-Institut für Medizinische Forschung,
Postfach 10 38 20, D-69028 Heidelberg, Germany
e-mail: vkitzing@sunny.MPImF-Heidelberg.mpg.de

Table 1 Comparing PNPC terminology in different fields[a]

	Biological ion channels	Ion exchange membranes	Semiconductors
Charge transport medium	Ion channel	Membrane	Semiconductor
Background charge density	Permanent charge density	Fixed charge density	Doping function
Negative background charge density	Cation channel	Cation exchanger	*p*-Semiconductor
Positive background charge density	Anion channel	Anion exchanger	*n*-Semiconductor
Positive mobile charge carriers	Cations	Cations	Holes
Negative mobile charge carriers	Anions	Anions	Electrons

[a] Gauss' or Poisson's law, Nernst-Planck, and continuity equations (PNPC) are introduced independently in several fields of diffusion-controlled charge transport. Each field developed its own terminology. Here we compare some terms relevant for biological ion channels, ion exchange membranes, and semiconductors

of thickness l between inhomogeneous interfaces, the system is internally close to electroneutral (MacGillivray 1967; Mafé et al. 1987; Barcilon et al. 1997; Chen et al. 1997). To describe charge transport through biological ion channels, often Eyring's absolute rate theory (Eyring et al. 1949; Laidler and King 1983; Hille 1992) or Kramers' theory (Kramers 1940; Cooper et al. 1985; Weiss 1986) are used where ion permeation is assumed to be determined by the presence of a few barriers and binding sites. In those theories the electrostatic interactions between permeant ions and permanent charges at the channel walls are generally not correctly taken into account (Eisenberg 1996; Nonner et al. 1998; Syganow and von Kitzing 1999).

Analytical solutions for long biological ion channels assuming negligible ion pairing (PNP) (Peskoff and Bers 1988; Levitt 1991a) are given in the limit of weak electric fields ($l_{DH}E \ll RT/F$). Approximate analytical solutions are constructed using singular perturbation methods (MacGillivray 1967; MacGillivray and Hare 1969; Barcilon et al. 1997; Park and Jerome 1997). The majority of calculations apply numerical methods (Offner 1971; Buck 1984; Mafé et al. 1986; Peskoff and Bers 1988; Levitt 1991b; Chen et al. 1992; Nonner and Eisenberg 1998). Brownian dynamic calculations represent an even more detailed picture of ion permeation (Ermak and McCammon 1978; Cooper et al. 1985; Bek and Jakobsson 1994; Chung et al. 1998). Numerical simulations have an advantage because they apply to complicated, realistic systems. They invent a minimal number of approximations; therefore numerical methods generally give the most reliable results. Computers are widely available; consequently those numerical approaches appear to be the most reasonable choices to study biological ion channels.

Numerical solutions, however, have a big disadvantage. It is not possible to distinguish between special and general properties of a model in order to understand the overall behavior of a certain class of ion channels and to derive the respective general rules. In addition, the number of free parameters seldom allows a scanning of the whole parameter space. On the other hand, approximate analytical solutions are often not sufficiently accurate to provide precise numbers, but at least they show qualitatively, often even quantitatively, the important kinds of solutions for a given situation. They show the typical classes of solutions of the problem under study. Particularly for the highly nonlinear PNPC equations it is important to understand the typical modes of behavior. Only if one has a fairly reasonable understanding of the kinds of solution to expect can one guess from experimental current-voltage curves the relevant ion transport mechanism, and can design the necessary experiments to discriminate between different mechanisms of ion transport.

We showed recently (Syganow and von Kitzing 1995) that solutions of the PNPC equations can be classified into three domains: the equilibrium domain, the diffusion domain, and the drift domain. In the drift domain the solutions are dominated by the electric field, and the current-voltage curves are close to linear. In this domain, the contribution of concentration gradients to the electric current density is small. It has been known for a long time in semiconductor physics that close to linear current-voltage curves indicate a drift ion transport mechanism (Schottky and Spenke 1939; Pekar 1941; Syganow and Swetchnikow 1981). Recently, *drift approximation* was proposed to explain ion permeation for long biological ion channels ($L > l_{DH}$) with nearly linear current-voltage curves (Syganow and von Kitzing 1995). For large external voltage ($V > RT/F$), drift approximation represents the exact limiting solution for the PNPC equations.

In this article we derive a simple analytical drift current-voltage relation, the voltage as a second-order polynomial of the electric current. We generalize the drift approximation derived by others to describe charge transport in semiconductors (Schottky and Spenke 1939; Lampert and Mark 1970; Syganow and Swetchnikow 1981; Sze 1981) to the fields of ion exchange membranes and biological ion channels. It is based on the drift limit of the complete set of PNPC equations where the electric field dominates the electric current. Under certain conditions given below, the coefficients of this polynomial can be calculated analytically. In the results section we apply the drift approximation to simple physical models of ion transport and compare the approximate analytical results with those obtained from numerical solutions of the complete set of PNPC equations. By means of the drift current-voltage relation, certain parameters of simple ion transport systems can be estimated directly from experimental data without the need of complex numerical simulations. We show that pairing is generally not negligible. The respective values of the association rate constants are estimated using diffusion limited reaction rate theory. In the discussion the assumptions introduced in the theory are critically analyzed. We discuss the importance of the continuity equation in the PNPC theory.

Theoretical methods

In this section we derive the drift current-voltage relation from Gauss' law, the drift, and continuity equations. The necessary condition to apply the drift approximation of the Nernst-Planck equation was given previously (Syganow and von Kitzing 1995). Although we repeatedly refer to the particular situation inside biological ion channels, the derivation of the drift current-voltage relation is entirely general and contains no assumption which limits its validity to such special systems.

First we express the external voltage formally as a second-order polynomial in the electric current. The coefficients of this polynomial, however, are still implicit functions of the current. We derive conditions under which these coefficients become constant. Finally, we present limiting cases for which the coefficients of this polynomial can be calculated analytically.

General basis for the drift approximation

In the *drift approximation*, ion fluxes are described by the drift, Gauss' or Poisson's, and the continuity equations. In the drift limit the influence of diffusion due to concentration gradients of permeant ions is small on integral quantities such as current-voltage relations (Syganow and von Kitzing 1995). The drift equation is given by:

$$\boldsymbol{j}(\boldsymbol{r}) = \sigma(\boldsymbol{r})\,\boldsymbol{E}(\boldsymbol{r}) \quad \text{with} \quad \nabla \boldsymbol{j} = 0 \tag{1}$$

where $\boldsymbol{j}$ is the total mean electric current density due to permeant ions (or any other kind of charge carriers) at the position $\boldsymbol{r}$ in space, $\sigma(\boldsymbol{r})$ is the specific conductivity, $\boldsymbol{E}$ is the mean electric field, and ∇ is the three-dimensional spatial derivative. In steady state the total current density is conserved, i.e., charges are neither created nor destroyed. Gauss' law relates the electric field to the mean electric charge density $\rho(\boldsymbol{r})$:

$$\nabla \boldsymbol{E} = \frac{\rho(\boldsymbol{r})}{\varepsilon_0\,\varepsilon}; \quad \text{and} \quad \boldsymbol{E} = -\nabla\phi(\boldsymbol{r}) \tag{2}$$

where ε_0 is the vacuum permittivity, ε the macroscopic dielectric constant, and ϕ the potential of the mean electric field $\boldsymbol{E}$. Equation (2) represents the differential form of Gauss' law for isotropic macroscopic media; together with the electric potential ϕ it leads to Poisson's law. Finally, we introduce the continuity equation:

$$2F\,\mathcal{R}(\boldsymbol{r}) = \nabla \boldsymbol{j}_n - \nabla \boldsymbol{j}_p \quad \text{and} \quad \boldsymbol{j} = \boldsymbol{j}_p + \boldsymbol{j}_n \tag{3}$$

where F is Faraday's constant, $\mathcal{R}$ is the ion pairing intensity, the rate of ion pairing in a unit volume, and $\boldsymbol{j}_p$ and $\boldsymbol{j}_n$ are the electric current densities of cations and anions, respectively. The continuity Eq. (3) accounts for ion pairing, i.e., the association and dissociation of oppositely charged permeable ions (Bockris and Reddy 1970; Oelkers and Helgeson 1993). For a vanishing ion pairing intensity $\mathcal{R}$, the continuity equation indicates the conservation of ion numbers. As shown below, pairing influences the dynamics of ion transport even if the concentration of pairs remains negligible. In Eq. (3), only two monovalent ion species are considered; however, this approach can be extended to any number of species and any combination of valencies.

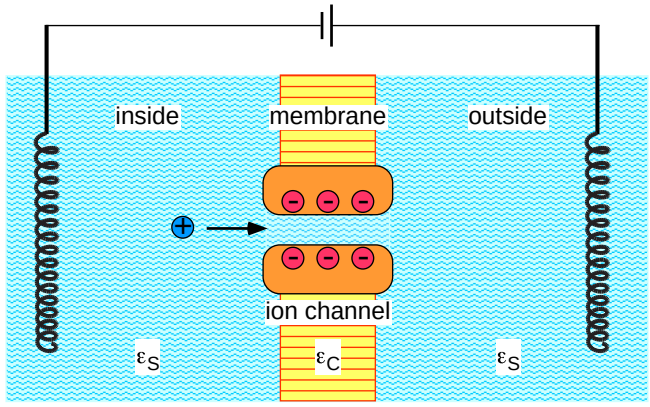

Fig. 1 Biological ion channels are proteins embedded in lipid membranes with a low dielectric constant ($\varepsilon_C \ll \varepsilon_S$). The permeability for ions of these channels is regulated, e.g., by a neurotransmitter or by the voltage difference across the membrane (Hoppe et al. 1982; Hille 1992). For instance, the acetylcholine receptor channel transmits the excitation of the neuron to the muscle fiber. The walls of the channel pore often contain charged amino acid side chains. Here, the channel is assumed to be long compared to its diameter. The terms "inside" and "outside" specify the situation in the living cell, to the cytoplasmatic and extra-cellular sides of the cell, respectively. As indicated by the *arrow*, the electric current is defined to be positive if cations leave the cell

The electric voltage V along the channel axis and the electric current I through the channel generally can be measured experimentally. It is therefore useful to express the complex behavior of Eqs. (1)–(3) in terms of I and V. They can be obtained by integrating the electric field E along the channel and the current density j over the channel's cross-section, respectively:

$$V(I) = \int_L \boldsymbol{E}\,\mathrm{d}\boldsymbol{r} \quad \text{and} \quad I = \int_S \boldsymbol{j}\,\mathrm{d}\boldsymbol{n} \tag{4}$$

where L is the length of the channel, S is the local cross-section of the channel, and $\boldsymbol{n}$ is the vector normal to the surface element. To be able to obtain analytical results we confine our analysis to the one-dimensional version of Eqs. (1)–(3). Therefore, our calculations apply to "sufficiently" one-dimensional systems such as permeable membranes, or cylindrical channels where the effective length L of the channel exceeds its diameter (see Fig. 1).

Drift current-voltage relations

In this section we integrate the three fundamental Eqs. (1)–(3) to obtain a formally simple *drift current-voltage relation* which can directly be compared with numerical

solutions of the full Poisson-Nernst-Planck equations (PNP) or experimental current-voltage curves. In the drift Eq. (1), the electric field E inside the channel is given as a function of the position z along the channel axis. By means of Eq. (1) the electric field E is redefined as function of the specific conductivity σ. We differentiate Eq. (1), apply the conservation of total electric charge $\mathrm{d}j/\mathrm{d}z = 0$, and replace E by j/σ:

$$\mathrm{d}E = -\frac{E}{\sigma}\,\mathrm{d}\sigma = -\frac{j}{\sigma^2}\,\mathrm{d}\sigma$$

Analogously, the position z inside the channel can be expressed in terms of the specific conductivity σ. We resolve Gauss' law (2) for $\mathrm{d}z$ and replace $\mathrm{d}E$ by the previous result:

$$\mathrm{d}z = \frac{\varepsilon_0\,\varepsilon}{\rho}\,\mathrm{d}E = \frac{\varepsilon_0\,\varepsilon\,j}{\rho\sigma^2}\,\mathrm{d}\sigma \tag{5}$$

A $z(\sigma)$ relation can be obtained from Gauss' law (2) as well as from the continuity Eq. (3). After introducing the specific cation and anion conductivities, σ_p and σ_n, respectively, with $\sigma = \sigma_p + \sigma_n$, the drift equations for individual ions takes the form: $j_{p/n} = \sigma_{p/n} E$. Now we rewrite the continuity Eq. (3):

$$\mathrm{d}z = \frac{\mathrm{d}j_n - \mathrm{d}j_p}{2F\mathcal{R}} = \frac{\mathrm{d}[(\sigma_n - \sigma_p)\,E]}{2F\mathcal{R}}$$
$$= -\frac{\mathrm{d}[\tilde{\sigma}\,E]}{2F\mathcal{R}} = -\frac{\tilde{\sigma}\,\mathrm{d}E + E\,\mathrm{d}\tilde{\sigma}}{2F\mathcal{R}}$$

where we define the specific conjugate conductivity $\tilde{\sigma} = \sigma_p - \sigma_n$. E and $\mathrm{d}E$ in this expression are substituted using the drift Eq. (1) or its derivative given above. With the prime $'$ indicating the σ derivation $\mathrm{d}/\mathrm{d}\sigma$, this result leads to a formulation of $\mathrm{d}z$ based on the continuity Eq. (3):

$$\mathrm{d}z = -\frac{\sigma\tilde{\sigma}' - \tilde{\sigma}}{2F\mathcal{R}\,\sigma^2}\;j\,\mathrm{d}\sigma \tag{6}$$

Equations (5) and (6) define a variable transformation: the z dependence of the specific conductivity $\sigma(z)$ is inverted into $z(\sigma)$. Such an inversion is only unique in intervals where the $\sigma(z)$ relation is monotonic. If $\sigma(z)$ contains extreme points we choose the inversion intervals such that the specific conductivity is monotone within each interval. In the example shown in Fig. 2, the specific conductivity has a single extremum σ_E at z_E, and the intervals for which the specific conductivity is monotone are $(z_\mathrm{i}, z_\mathrm{E})$ and $(z_\mathrm{E}, z_\mathrm{o})$. After variable transformation the charge density $\rho(z)$ and the pairing intensity $\mathcal{R}(z)$ are functions of the specific conductivity σ, i.e., $\rho(\sigma)$ and $\mathcal{R}(\sigma)$. For simplicity, this dependence is omitted in the formulae.

To obtain a drift current-voltage relation, we integrate $\mathrm{d}z$ and $E\,\mathrm{d}z$, leading to the channel length L and the external voltage V, respectively. This integration is performed using both formulations of $\mathrm{d}z$ in Eqs. (5) and (6). The electric field E is substituted using the drift Eq. (1):

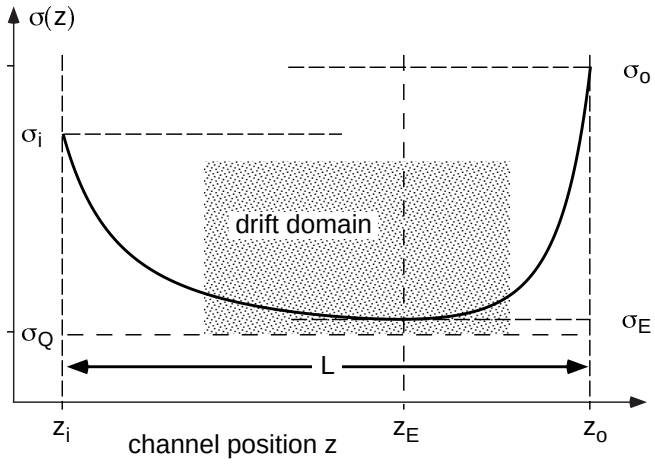

Fig. 2 The specific conductivity profile for a simple charge transport model, such as a biological ion channel (see Fig. 1). This curve was taken from the numerical solution of the full Poisson-Nernst-Planck equations with an external voltage of $V = 150$ mV and $L/l_\mathrm{DH} = 5$ with the channel length L and a Debye length l_DH. The equilibrium specific conductivity of σ_Q corresponds to the conductivity of very long channels. For instance, in the case of $L/l_\mathrm{DH} = 20$ the minimal specific conductivity σ_E deviates from σ_Q less than 1%. Here, the specific conductivity $\sigma(z)$ has a single minimum $\sigma_\mathrm{E}/\sigma_\mathrm{Q} \approx 5/4$ at z_E. The channel region extends from the intracellular electrolyte solution with a specific conductivity of $\sigma_\mathrm{i}/\sigma_\mathrm{Q} = 4$ at z_i to the extracellular solution at z_o with $\sigma_\mathrm{o}/\sigma_\mathrm{Q} = 5$. The drift domain of the solution of the PNPC set of equations prevails in the *dotted interval*. Because the channel conductance is determined by the domain inside the channel where the conductivity is smallest, for the situation shown in this figure, ion transport can be well approximated by a drift ion transport mechanism (see results)

$$L = \int_0^L \mathrm{d}z \approx -\varepsilon_0\,\varepsilon\,j \int_{\sigma_\mathrm{i}}^{\sigma_\mathrm{o}} \frac{\mathrm{d}\sigma}{\rho\sigma^2} = -\frac{j^2}{2F} \int_{\sigma_\mathrm{i}}^{\sigma_\mathrm{o}} \frac{\sigma\tilde{\sigma}' - \tilde{\sigma}}{\mathcal{R}\,\sigma^2}\,\mathrm{d}\sigma$$
$$V = \int_0^L E\,\mathrm{d}z \approx -\varepsilon_0\,\varepsilon\,j^2 \int_{\sigma_\mathrm{i}}^{\sigma_\mathrm{o}} \frac{\mathrm{d}\sigma}{\rho\sigma^3} = -\frac{j^2}{2F} \int_{\sigma_\mathrm{i}}^{\sigma_\mathrm{o}} \frac{\sigma\tilde{\sigma}' - \tilde{\sigma}}{\mathcal{R}\,\sigma^3}\,\mathrm{d}\sigma \tag{7}$$

where σ_i and σ_o are specific conductances at the channel boundaries, as indicated in Fig. 2. Because we replace $\mathrm{d}z$ by its drift approximation, these relations are not exact but apply in the drift limit.

From the equations for the channel length L and the voltage V, we derive the drift current-voltage relation. First we consider a linear relationship. For long homogeneous channels at equilibrium, the specific conductivity is close to the equilibrium specific conductivity σ_Q. Consequently, the respective current-voltage relation has the form of Ohm's law: $V = jL/\sigma_\mathrm{Q}$. By introducing Ohm's law into the voltage in Eq. (7), we formulate the limiting form of the current-voltage relation for long channels where the deviation of the specific conductivity at z_i and z_o from the equilibrium conductivity σ_Q has a negligible influence on the channel conductance Σ. Thus, the remaining integrals must become small in this limit. Adding Ohm's term jL/σ_Q to the voltage V and substracting it using both integral forms of L in Eq. (7) leads to the relation:

$$V = \frac{j\,L}{\sigma_Q} + \frac{\varepsilon_0\,\varepsilon\,j^2}{\sigma_Q}\int_{\sigma_i}^{\sigma_o}\frac{\sigma-\sigma_Q}{\rho\sigma^3}\,d\sigma$$

$$= \frac{j\,L}{\sigma_Q} + \frac{j^2}{2F\,\sigma_Q}\int_{\sigma_i}^{\sigma_o}[\sigma\tilde{\sigma}'-\tilde{\sigma}]\frac{\sigma-\sigma_Q}{\mathcal{R}\,\sigma^3}\,d\sigma \qquad (8)$$

Formally, Eq. (8) represents the external voltage V as a second-order polynomial of the current density j. The extreme specific conductivity σ_E, which appears in the boundaries of the path integral, generally is a function of the current density. Consequently, the integrals in Eq. (8) still depend on j, but σ_E becomes constant in the low current limit (see below).

Now, we replace the current density j by the experimentally accessible electric current $I=Sj$, and include the integrals in the characteristic current I_c. Thus, I_c describes the deviation of the current-voltage relation from linearity. This leads to the formally simple *drift current-voltage relation*:

$$V = V_D + \frac{I}{\Sigma}\left[1-\frac{I}{I_c}\right] \quad \text{with} \quad \Sigma = \frac{S}{L}\sigma_Q \qquad (9)$$

The diffusion voltage V_D is not derived from drift approximation (8), but from a more general approach (Syganow and von Kitzing 1995), and it is added here for completeness. The diffusion potential V_D should not be mistaken for the reversal potential $V_R(I=0)$, because the approximation of Eq. (9) applies only at large voltages. Σ is the drift conductance of the channel. The characteristic current I_c yields:

$$I_c = \frac{S\,L}{\varepsilon_0\,\varepsilon}\sigma_Q\,\rho_c = F\,S\,L\,\mathcal{R}_c \qquad (10)$$

The characteristic current I_c is expressed either via the characteristic charge density ρ_c or the characteristic pairing intensity $\mathcal{R}_c$ representing the two integrals in Eq. (8):

$$\frac{1}{\rho_c} = \sigma_Q\int_{\sigma_i}^{\sigma_o}\frac{\sigma-\sigma_Q}{\rho\sigma^3}\,d\sigma$$

and

$$\frac{1}{\mathcal{R}_c} = \frac{1}{2}\int_{\sigma_i}^{\sigma_o}[\sigma\tilde{\sigma}'-\tilde{\sigma}]\frac{\sigma-\sigma_Q}{\mathcal{R}\,\sigma^3}\,d\sigma \qquad (11)$$

To calculate the characteristic charge density ρ_c or the characteristic pairing intensity $\mathcal{R}_c$, we need $\rho(\sigma)$ and $\mathcal{R}(\sigma)$ as explicit functions in σ. Such explicit channel models are considered below.

From the characteristic current I_c and the drift conductance Σ, we calculate the *characteristic voltage*. Inversion of the current-voltage Eq. (9) leads to the current as a function of the external voltage:

$$V_c = \frac{I_c}{\Sigma} \quad \text{with} \quad I(V) = \frac{I_c}{2}\left(1-\sqrt{1-4\,\frac{V-V_D}{V_c}}\right) \qquad (12)$$

The characteristic voltage denotes the ion transport mechanism. Small characteristic voltages $V_c \approx RT/F$ indicate equilibrium or diffusion solutions of the PNPC equations (Syganow and von Kitzing 1995). Drift approximation, however, predicts much larger characteristic voltages with $V_c \gg RT/F$.

Characteristic current

By introducing Ohm's law for long systems into the drift current-voltage relation (9), we included all the difficult parts of this relation in the characteristic current I_c. To calculate I_c we first consider the limits of weak and strong ion-pairing. This directly leads to explicit relationships between the charge density ρ or the recombination intensity $\mathcal{R}$ and the specific conductivity σ needed to estimate the characteristic charge density ρ_c or the pairing intensity $\mathcal{R}_c$. The calculation of the characteristic current can be further simplified by using the fact that only one half of the integrals of ρ_c and $\mathcal{R}_c$ in Eq. (11) contribute significantly in the drift limit (Syganow and von Kitzing 1995). For electric currents below a critical current I_c^*, the extreme specific conductivity σ_E becomes independent of the current I. This leads to a current-independent characteristic current I_c.

Weak and strong ion pairing

To obtain simple relations between ρ, $\mathcal{R}$, and σ, we introduce the limits of weak and strong ion pairing. In Eq. (7) the external voltage V and the channel length L are calculated either from a combination of the drift Eq. (1) and Gauss' law (2) or from a combination of the drift and continuity Eqs. (1) and (3). As long as no further approximations are introduced, both formulations are equivalent. Equating $dz/d\sigma$ in Eqs. (5) and (6) results in a first-order, nonlinear differential equation relating the charge density $\rho(\sigma)$ and the pairing intensity $\mathcal{R}(\sigma)$:

$$2F\,\varepsilon_0\,\varepsilon_C\,\mathcal{R} = [\tilde{\sigma}-\sigma\tilde{\sigma}']\,\rho \qquad (13)$$

For steady state homogeneous systems, Eq. (13) holds trivially, because ρ and $\mathcal{R}$ vanish. Generally $\tilde{\sigma}-\sigma\tilde{\sigma}'$ is nonzero. We do not know any analytic solution for Eq. (13), except for very long systems with a negligible equilibrium specific conductivity ($\sigma_Q \ll \sigma$) (Parmenter and Ruppel 1959). One can, however, distinguish two limiting cases: the quasi-neutral limit with $\rho \approx 0$ and the space-charge limit with $\mathcal{R} \approx 0$. Which of the two cases applies, depends critically on the actual model parameters determining pairing.

In the presence of anions and cations, the total charge density ρ consists of positive ρ_p as well as negative contributions ρ_n with $\rho=\rho_p-\rho_n$. If the two charge contributions are large but nearly cancel the *quasi-neutral drift ion transport mechanism* dominates:

$$\rho_p \approx \rho_n \gg |\rho| = 2F\,\varepsilon_0\,\varepsilon_C\left|\frac{\mathcal{R}}{\tilde{\sigma}-\sigma\tilde{\sigma}'}\right| \qquad (14)$$

This condition implies that the total charge density is generally close to zero ($\rho \approx 0$). Such electroneutrality condition was introduced by Planck (Planck 1890) a long time ago. The total charge density becomes small for small association rate constants k_A which makes $\mathcal{R}$ small due to $\mathcal{R} \propto k_A$ (see below). In this case the right hand side of this equation will generally be small, implying a small total charge density ρ. In semiconductor physics, this limit is designated the *recombination limited case* (Stöckmann 1961; Lampert and Mark 1970).

Similarly, the pairing intensity $\mathcal{R}$ is composed of an association term $\mathcal{R}_a$ and a dissociation term $\mathcal{R}_d$ with $\mathcal{R} = \mathcal{R}_a - \mathcal{R}_d$. For large ion association rate constants k_A the association term $\mathcal{R}_a$ and the dissociation term $\mathcal{R}_d$ are generally large. To match the charge density ρ in Eq. (13) they must be similar in magnitude, because a large charge density would be energetically unfavorable. Under this condition the *space-charge drift ion transport mechanism* is obtained:

$$\mathcal{R}_a \approx \mathcal{R}_d \gg |\mathcal{R}| = \left| \frac{\tilde{\sigma} - \sigma \tilde{\sigma}'}{2 F \varepsilon_0 \varepsilon_C} \rho \right| \tag{15}$$

In semiconductor physics, this limit is designated the *space-charge limited case* (Stöckmann 1961; Lampert and Mark 1970).

Starting from Eq. (13) we derived the quasi-neutral and the space-charge ion transport mechanisms. Relations (14) and (15), respectively, indicate one of those mechanisms. For particular relations between the charge density ρ, the ion pairing intensity $\mathcal{R}$, and the cation p and anion concentrations n, these limiting situations lead to explicit expressions for ρ and $\mathcal{R}$. Further below, we consider such explicit models where approximate characteristic currents I_c can be calculated analytically.

Simplifying the characteristic currents

The integrals in Eq. (8) are path-integrals and have to be taken along the channel axis. In this article we consider channels containing a single extremum σ_E of the specific conductivity (see Fig. 2). This extremum at z_E splits the path-integrals into two halves. The integrals have to be evaluated using the bounds of $\int_{\sigma_i}^{\sigma_E}$ and $\int_{\sigma_E}^{\sigma_o}$. This splitting up of the integrals $\int_{\sigma_i}^{\sigma_o}$ for ρ_c and $\mathcal{R}_c$ has the advantage that, in the drift limit for each of the two limiting ion transport mechanisms, one of the two parts of the integrals $\int_{\sigma_i}^{\sigma_E}$ or $\int_{\sigma_E}^{\sigma_o}$ becomes small and can be neglected. The choice which of the two parts becomes small depends on the sign of the external voltage and the kind of the ion transport mechanism. For strong pairing and positive external voltages the second integral becomes small compared to the first one and can, therefore, be neglected (Syganow and von Kitzing 1995):

$$\int_{\sigma_i}^{\sigma_o} \frac{\sigma - \sigma_E}{\rho \sigma^3} \, d\sigma \approx - \int_{\sigma_E}^{\sigma_i} \frac{\sigma - \sigma_E}{\rho \sigma^3} \, d\sigma$$

Analogously, for weak ion pairing and positive external voltages the first integral becomes small compared to the second one. For negative external voltages the opposite choice for the integral boundaries must be taken.

The low current limit

In addition to an explicit relation between ρ, $\mathcal{R}$, and σ, the calculation of the characteristic current I_c requires estimates for the extreme conductivity σ_E. Here we show that for not too large currents I this extreme specific conductivity σ_E is close to the equilibrium specific conductivity σ_Q inside the channel. We obtain this relation from the integral for the channel length L in Eq. (7). For a first estimate we use a first-order Taylor series of the charge density ρ around the equilibrium specific conductivity σ_Q. For particular models with explicit expressions for $\rho(\sigma)$ this approximation becomes unnecessary (see below). With $I = Sj$ and $\rho(\sigma) \approx \rho'_Q(\sigma - \sigma_Q)$ the channel length L becomes:

$$L \approx \frac{\varepsilon_0 \varepsilon I}{S} \int_{\sigma_E}^{\sigma_i} \frac{d\sigma}{\rho \sigma^2} \approx \frac{\varepsilon_0 \varepsilon I}{S \rho'_Q} \int_{\sigma_E}^{\sigma_i} \frac{d\sigma}{(\sigma - \sigma_Q)\sigma^2}$$
$$= \frac{\varepsilon_0 \varepsilon I}{S \rho'_Q \sigma_Q^2} \left\{ \frac{\sigma_Q}{\sigma} + \ln\left[1 - \frac{\sigma_Q}{\sigma}\right] \right\}_{\sigma_E}^{\sigma_i}$$

The channel length is always positive; consequently, the right hand side of this equation must also be positive. Therefore, we can include all the constants in a positive, critical current I_c^*. If I_c^* appears to be negative, L might also be negative, and the choice of the boundary specific conductivities should be reconsidered. For instance, for negative currents the correct integral takes the form $-\int_{\sigma_E}^{\sigma_o}$. With the critical current the Taylor approximation of the length integral can be rewritten:

$$1 \approx - \frac{2I}{I_c^*} \left\{ \frac{\sigma_Q}{\sigma_E} - \frac{\sigma_Q}{\sigma_i} + \ln\left[\frac{\sigma_i}{\sigma_E} \frac{\sigma_E - \sigma_Q}{\sigma_i - \sigma_Q} \right] \right\}$$

$$\text{with} \quad I_c^* = 2SL \frac{\sigma_Q^2 |\rho'_Q|}{\varepsilon_0 \varepsilon_C} \tag{16}$$

At small electric currents with $2|I|/I_c^* \ll |\sigma_Q/\sigma_E - \sigma_Q/\sigma_i|$ the ln-term must become large such that the right hand side yields unity. This in turn implies:

$$\left| \frac{\sigma_Q}{\sigma_E} - \frac{\sigma_Q}{\sigma_i} \right| \ll \left| \ln\left[\frac{\sigma_i}{\sigma_E} \frac{\sigma_E - \sigma_Q}{\sigma_i - \sigma_Q} \right] \right|$$

Consequently, the term $\sigma_Q/\sigma_E - \sigma_Q/\sigma_i$ can be neglected in Eq. (16). Here we explicitly need that the critical current I_c^* is always positive. Otherwise, the ln-term would not necessarily outweigh the other terms in Eq. (16). This leads to an expression for σ_E as a function of the electric current which applies for small currents ($|I| < I_c^*/2$):

$$\sigma_E \approx \frac{\sigma_Q}{1 - [1 - \sigma_Q/\sigma_i] \exp[-I_c^*/(2I)]} \tag{17}$$

The neglected term $\sigma_Q/\sigma_E - \sigma_Q/\sigma_i$ contributes at $I \approx I_c^*/2$ and above. When the total current I approaches the critical current I_c^* the specific conductivity σ in the channel becomes increasingly determined by its boundary values. The minimal concentration σ_E starts to deviate considerably from the equilibrium concentration σ_Q owing to injected ions. Consequently, the characteristic current I_c in the drift current-voltage relation (9) becomes independent of the electric current in the limit of low currents ($|I| \ll I_c^*/2$). Because the minimal conductivity σ_E in Eq. (17) depends exponentially on I_c^*, the convergence towards σ_Q is obtained rather quickly for $|I| < I_c^*/2$. For negative currents, σ_i in Eq. (17) must be replaced by σ_o and the "–" sign in the exponential function by "+".

The quasi-neutral equivalent to the space-charge critical current I_c^* is calculated analogously, yielding:

$$I_c^* = 2 \left| \frac{FSL\sigma_Q^2 \mathcal{R}'_Q}{\tilde{\sigma}_Q - \sigma_Q \tilde{\sigma}'_Q} \right| \tag{18}$$

The order of the values of the characteristic current I_c and the critical current I_c^* are similar. The drift current-voltage relation for positive I_c is unique only for $-|I_c| < 2I < +|I_c|$. Thus, the drift current-voltage relations limits the amplitude of the electric current analogously as the critical current I_c^*. Below, we introduce explicit models ρ and $\mathcal{R}$ and we calculate the critical current directly without the approximation of $\rho \approx \rho'_Q(\sigma - \sigma_Q)$ and $\mathcal{R} \approx \mathcal{R}'_Q(\sigma - \sigma_Q)$. In all models of diffusion-controlled ion transport considered in this article, the critical and characteristic currents are of the same order of magnitude.

Characteristic charge density and pairing intensity

Thus, for electric currents below the critical current ($I_c^*/2 \gg I$), the extreme specific conductivity σ_E at z_E is close to the equilibrium specific conductivity σ_Q. Consequently, the integrals for the characteristic charge density ρ_c and the characteristic pairing intensity $\mathcal{R}_c$ in Eq. (9) are further simplified by replacing σ_E by σ_Q:

$$\rho_c^{-1} \approx \pm\sigma_Q \int_{\sigma_Q}^{\sigma_{o/i}} \frac{\sigma - \sigma_Q}{\rho\sigma^3}\, d\sigma$$

and

$$\mathcal{R}_c^{-1} \approx \mp\frac{1}{2} \int_{\sigma_Q}^{\sigma_{o/i}} [\sigma\tilde{\sigma}' - \tilde{\sigma}] \frac{\sigma - \sigma_Q}{\mathcal{R}\sigma^3}\, d\sigma \tag{19}$$

In the general case, the same characteristic current I_c is obtained independent of whether the characteristic charge density ρ_c or the characteristic pairing intensity $\mathcal{R}_c$ in Eqs. (9)–(11) are used. After introducing the limits for the space-charge and quasi-neutral ion transport mechanisms, either ρ_c or $\mathcal{R}_c$ as defined in Eq. (19), respectively, must be used to calculate I_c. After that limit has been applied, the two versions of the characteristic current I_c differ, because the smaller term, $\mathcal{R}$ or ρ, is approximated by zero.

Simple models for the ion permeation path

In this section we apply the drift current-voltage relation given in Eqs. (9)–(11) to simple models of diffusion-controlled ion transport. To keep the article short, only the simplest possible models are analyzed. More complex models, e.g., including binding of ions to charged amino acid side chain, can be calculated accordingly. To show the validity of our approximations, we compare the analytical result valid in the drift limit with numerical solutions of the complete set of PNPC equations.

Below, first we set up the model equations expressing σ, $\tilde{\sigma}$, ρ, and $\mathcal{R}$ as functions of the cation p and anion concentrations n. The ion association rate constant k_A, which appears in the continuity equation, is estimated from modern reaction rate theories. Than we calculate the characteristic current I_c for models assuming space-charge conduction mechanisms and compare it with numerical results. Finally, we explore the quasi-neutral conduction mechanisms.

Fundamental model equations

To calculate the characteristic current I_c as given by Eqs. (10) and (19), we express the specific conductivity σ, the specific conjugate conductivity $\tilde{\sigma}$, the charge density ρ, and the pairing intensity $\mathcal{R}$ in terms of cation and anion concentration p and n:

$$\begin{aligned} \sigma(z) &= F[u_p\, p(z) + u_n\, n(z)] \\ \tilde{\sigma}(z) &= F[u_p\, p(z) - u_n\, n(z)] \\ \rho(z) &= F[p(z) - n(z) - N] \end{aligned} \tag{20}$$

where u_p and u_n are the mobilities of permeant cations and anions, respectively. $p(z)$ and $n(z)$ are the respective concentrations of free, unbound ions. For convenience the channel conductance is assumed to be dominated by cations. Therefore, only permanent negative charges are considered inside the channel. N is the concentration of the negative charge density, taken to be constant. In biological ion channels, such permanent charge density originates from charged amino acids that form the wall of the channel pore. At conditions used to define the equilibrium specific conductivity σ_Q or the respective concentrations p_Q and n_Q, the channel must be neutral: $N = p_Q - n_Q$.

To account for pairing between cation and anions, we introduce a simple reaction rate equation:

$$\mathcal{R} = k_A\, pn - k_D c_Q = k_A(pn - p_Q n_Q) \tag{21}$$

where k_A is the ion association rate constant among permeant ions, k_D the respective dissociation rate constant, and c_Q the equilibrium concentration of ion pairs. We assume that k_D and c_Q are constant. With $k_D c_Q = k_A p_Q n_Q$, the second form of the pairing equation is obtained, omitting c_Q and k_D. Replacing them by p_Q and n_Q conveniently simplifies the resulting equations, because p_Q and n_Q are directly related to the channel's electrical properties.

Association rate constant

The pairing intensity $\mathcal{R}$ as given by Eq. (21) contains the association rate constant k_A as a material constant. Together with the dielectric constant ε_C inside the channel, this parameter determines the ion transport mechanism of the channel due to condition (15) for the space-charge or condition (14) for the quasi-neutral transport mechanism. It is therefore important to know at least its order of magnitude.

Theories of diffusion controlled association are well established in chemistry (Calef and Deutch 1983). The association rate for cations and anions is given by (Sridharan et al. 1989):

$$k_A = 4\pi \frac{RT}{F} N_A (u_p + u_n) r_A \tag{22}$$

with

$$\frac{l_C}{r_A} = \int_1^\infty \frac{e^{-\psi(\lambda)}}{\lambda^2} d\lambda$$

where r_A is the effective association radius. N_A is Avogadro's number, $\lambda = r/l_C$ is the distance between the two ions scaled by the distance of closest approach l_C, and $\psi(\lambda)$ is the effective potential energy between the two ions divided by RT. Very similar results are obtained for rates of diffusion-controlled electron-hole annihilation in semiconductors (Pekar 1950; Rose 1978).

The potential $\psi(\lambda)$ in the integral of Eq. (22) is typically the Debye-Hückel potential, but even more complex theories give similar results (Sridharan et al. 1989). In this form the integral cannot be solved analytically. A reasonable approximation of this integral can be obtained if the Debye-Hückel potential is replaced by a shift Coulomb potential in the range of l_C to $l_C + \alpha l_{DH}$ and zero potential beyond $l_C + \alpha l_{DH}$:

$$\psi(\lambda, \alpha) \approx \begin{cases} \frac{l_{Bj}}{l_C}\left[\frac{1}{\lambda} - \frac{l_C}{l_C + \alpha l_{DH}}\right] & \text{for } 1 \le \lambda \le 1 + \alpha l_{DH}/l_C \\ 0 & \text{elsewhere} \end{cases}$$

where the Bjerrum length l_{Bj} defines the distance of the two ions where the interaction energy of the Coulomb potential equals thermal energy RT. The Coulomb potential is shifted to obtain zero potential at the cutoff at $l_C + \alpha l_{DH}$. α is a scaling parameter which should be in the range of $1 \le \alpha \le 2$. Substituting this ψ into Eq. (22) leads to an approximate effective association radius r_A where the integral can be solved analytically. For simplicity a 1:1 electrolyte is considered:

$$\frac{1}{r_A} \approx \frac{1}{l_{Bj}}\left(1 - \exp\left[-\frac{\alpha l_{DH}\, l_{Bj}}{(l_C + \alpha l_{DH})\, l_C}\right]\right) + \frac{1}{l_C + \alpha l_{DH}} \tag{23}$$

with

$$l_{Bj} = \frac{F^2}{4\pi \varepsilon_0 \varepsilon_C N_A RT} \quad \text{and} \quad l_{DH} = \sqrt{\frac{RT \varepsilon_0 \varepsilon_C}{F^2 (p_Q + n_Q)}}$$

For large Debye lengths ($l_{DH} \gg l_{Bj}$) the scaling parameter α should be close to unity; in the opposite case it should be closer to 2. For $\alpha = 7/5$ the relative error of the association rate constant $\Delta k_A/k_A$ between the result of Eq. (23) and the numerically solved exact solution is below 2% for $1 \le l_{DH}/l_{Bj} \le 10$ and below 40% for $1/10 \le l_{DH}/l_{Bj} \le 10$ for $0 \le l_{Bj}/l_C \le 100$. Some typical values for the effective association radius are given in Table 2. Because in this article the association rate constant k_A is only required to the order of magnitude, even a deviation of 40% is tolerable.

The classic result of Smoluchowski (1917) with $r_A \approx l_C$ is obtained if the product of the Bjerrum and Debye lengths is small compared to the squared distance of closest approach, i.e., in the limit of strong screening. If the Bjerrum and Debye lengths exceed the distance of closest approach, the effective association radius becomes the Bjerrum length: $r_A \approx l_{Bj}$.

Using the Bjerrum length defined in Eq. (23), the association rate constant from Eq. (22) can be reformulated:

$$k_A = F \frac{u_p + u_n}{\varepsilon_0 \varepsilon_C} \frac{r_A}{l_{Bj}} \tag{24}$$

Estimates of the distance of closest approach l_C for alkali-halide ions from fitting thermodynamic properties of these electrolytes using the MSA theory (Blum 1980) are in the range of 0.3–0.8 nm (Triolo et al. 1976; Ebeling and Scherwinski 1983; Soumpasis 1984). According to Table 2, the effective association radius is small ($r_A \ll l_{Bj}$) for large Bjerrum lengths with $l_{Bj}^2 \gg l_C l_{DH}$. This is the situation inside biological ion channels. In water, the effective association radius r_A and the Bjerrum length are of similar order.

Table 2 Typical Bjerrum, Debye, and effective association radii[a]

l_C	ε	l_{Bj}	l_{DH}		r_A			
					0.3 nm		0.8 nm	
Conc.			1 M	10 mM	1 M	10 mM	1 M	10 mM
	80	0.72	0.304	3.04	0.412	0.685	0.841	1.07
	20	2.88	0.152	1.52	0.437	1.32	0.854	1.51
	10	5.76	0.107	1.07	0.418	1.37	0.855	1.65
	5	11.5	0.076	0.76	0.393	1.22	0.852	1.6
	2	28.8	0.0481	0.481	0.363	0.941	0.843	1.4

[a] Typical Bjerrum, Debye, and effective association radii for the situation in biological ion channels and ion exchange membranes. To get the range of Bjerrum and Debye lengths together with the corresponding effective association radii r_A, these numbers were calculated for typical conditions in solution and inside the channel. All lengths are given in nm for a range of permittivities between 2 as a lower limit and 80 for the water environment. The Debye lengths are calculated at concentrations of 1 M and 10 mM. The distances of closest approach l_C are 0.3 nm and 0.8 nm. All lengths are calculated for a temperature of 290 K

Analytic space-charge ion transport mechanism

The intuitively simplest case is the space-charge transport mechanism, where pairing is fast compared to the electrical relaxation corresponding to a large association rate constant k_A. This case also applies to the monopolar approximation where only a single permeant species (e.g., cations or holes) exists. In this particular case, permeant counter charges are absent and cannot enforce a quasi-neutral situation. Pairing between permeant charges is excluded in this case, and drift charge transport is determined only by the drift Eq. (1) and Gauss' law (2).

Monopolar approximation

The case of a single permeant ion is designated the *monopolar approximation*. One of the two concentrations in Eq. (20) is set to zero; here we consider only permeant cations. Obviously, such a model excludes pairing between permeant ions, and the reaction rate equation (21) does not apply. The characteristic and critical currents are calculated using the charge density. With these assumptions the basic Eqs. (20) are replaced by:

$$\sigma = F u_p p \quad \text{and} \quad \rho = F(p - N) = (\sigma - \sigma_Q)/u_p$$

Now we calculate the critical current I_c^* to see whether the characteristic current I_c is sufficiently independent from the electric current I. For the monopolar approximation in the space-charge limit the charge density ρ is a linear function in the specific conductivity σ. Consequently, the Taylor expansion of the charge density ρ used to estimate I_c^* in Eq. (16) leads to the exact result and the critical current becomes:

$$I_c^* = 2SL\,\frac{\sigma_Q^2\,\rho'_Q}{\varepsilon_0\,\varepsilon_C} = \frac{2F^2\,SL}{\varepsilon_0\,\varepsilon_C}\,u_p\,p_Q^2 \tag{25}$$

The characteristic charge density ρ_c and the current I_c are calculated using Eqs. (19) and (10):

$$\rho_c = 2F\,p_Q = 2\sigma_Q/u_p \quad \text{and} \quad I_c = \frac{2F^2\,SL}{\varepsilon_0\,\varepsilon_C}\,u_p\,p_Q^2 \tag{26}$$

In this simple example the characteristic current I_c equals the critical current I_c^*. Thus, the low current approximation applies as long as the external voltage V remains considerably below the characteristic voltage V_c defined by Eq. (12).

Quasi-monopolar approximation

In the *quasi-monopolar approximation* two permeant ions are considered. The channel conductance is assumed to be dominated by the presence of a single ion species, e.g. the cations. The concentration of the anions n is determined by $\mathcal{R} \approx 0$ as a function of the cation concentration p using Eq. (21):

$$n = p_Q\,n_Q/p \tag{27}$$

The specific conductivity σ and the charge density ρ are given in Eq. (20).

We start with the condition for the space-charge transport mechanism [Eq. (15)], and express σ, $\tilde{\sigma}$, and ρ as functions of p only, using Eqs. (20), (21), and (27). The association rate constant is taken from Eq. (24). This leads to the condition for a space-charge transport mechanism for the quasi-monopolar approximation:

$$\frac{r_A}{l_{Bj}} \gg \frac{2u_p\,u_n}{u_p + u_n}\left|\frac{(p - p_Q)(p + n_Q)}{u_p\,p^2 - u_n\,p_Q\,n_Q}\right| \tag{28}$$

The cation concentration p covers the range from external cation concentration p_i and p_o to equilibrium concentration p_Q. For the space-charge transport mechanism the root in the denominator of this condition should be non-zero within this range. This situation is realized for a channel with $p_i \geq p \geq p_Q \geq n_Q$ and $u_n < u_p$. The condition for the space-charge transport mechanism is nearly trivially fulfilled if $u_p \gg u_n$. In this case, the permeant anions act as an immobile, inhomogeneous charge density.

As a next step we calculate the characteristic current I_c^*. For the quasi-monopolar approximation the charge density is no longer a linear function in p owing to the relation between n and p given in Eq. (27). Therefore, we evaluate the length integral used to define the critical current I_c^* [Eq. (16)] with the correct charge density ρ from Eqs. (20) and (27). To keep the result simple, we additionally assume a zero background charge density, resulting in $n_Q = p_Q$. In this case the characteristic current I_c^* and the minimal concentration at low currents becomes:

$$I_c^* = \frac{2F^2\,SL}{\varepsilon_0\,\varepsilon_C}\,\frac{(u_p + u_n)^2}{u_p - u_n}\,p_Q^2$$

and

$$p_E \approx p_Q\,\sqrt{\frac{1 + \dfrac{u_n}{u_p}\,e^{-I_c^*/(2I)}}{1 - e^{-I_c^*/(2I)}}}$$

Now we calculate the characteristic current. From Eq. (19) with $n_Q = p_Q$ we obtain the following inverse characteristic charge density:

$$\rho_c^{-1} = \left\{3 + u + \frac{[1 + u(u-6)]\arctan\sqrt{u}}{\sqrt{u}} + 2(u-1)\ln\left[\frac{4}{1+u}\right]\right\}\Big/\,[4F\,p_Q(1+u)]$$

with $u = u_n/u_p$. In the limit of small u the characteristic charge density ρ_c and the characteristic current I_c become:

$$\rho_c(u_n \ll u_p) \approx \frac{F\,p_Q}{1 - \ln 2} \quad \text{and} \quad I_c(u_n \ll u_p) \approx \frac{F^2\,SL}{\varepsilon_0\,\varepsilon_C}\,\frac{u_p\,p_Q^2}{1 - \ln 2}$$

As expected, the critical and characteristic currents for the quasi-monopolar approximation in the space charge limit are similar with each other and similar to those of the monopolar approximation.

Quasi-neutral ion transport mechanism

Now the quasi-neutral ion transport mechanism is considered, which requires at least two mobile ion species for pairing. This mechanism applies if the ion association rate k_A is small. In the quasi-neutral limit the Maxwell relaxation of the ion distribution is fast compared to the process of ion pairing.

We use the quasi-neutral condition (14), which leads to $\rho \approx 0$, to define a relation between n and p:

$$n \approx p - p_Q + n_Q \tag{29}$$

Thus, the specific conductivity σ, its conjugate $\tilde{\sigma}$, and the pairing intensity $\mathcal{R}$ are again functions of the cation concentration p only.

First, we calculate the condition for the quasi-neutral limit, starting from Eq. (14). σ and $\tilde{\sigma}$ are defined in Eq. (20) and $\mathcal{R}$ in Eq. (21). We use Eq. (29) to substitute n. The association rate constant k_A is taken from Eq. (24). For the quasi-monopolar quasi-neutral ion transport mechanism the following condition must hold:

$$\frac{r_A}{l_{Bj}} \lll \frac{u_p u_n}{(u_p + u_n)^2} \left| \frac{p(p_Q - n_Q)}{(p - p_Q)(p + n_Q)} \right| \tag{30}$$

where the background charge density $N = p_Q - n_Q$ must be non-zero to make the quasi-neutral limit possible. In contrast to the condition for a space-charge ion transport mechanism [Eq. (28)], the quasi-neutral limit requires similar ion mobilities, i.e. $u_p \approx u_n$. Condition (30) becomes easy to obey at cation concentrations close to its equilibrium concentration of $p \approx p_Q$. At concentrations very different from the equilibrium concentration a strict neutrality no longer holds.

To calculate the critical current we have to solve the integral for the channel length taken from Eq. (7):

$$L = -\frac{I}{2FS} \int_{\sigma_E}^{\sigma_o} \frac{\sigma \tilde{\sigma}' - \tilde{\sigma}}{\mathcal{R} \sigma^2} \, \mathrm{d}\sigma$$

This leads to a critical current I_c^* and limiting minimal concentration p_E of:

$$I_c^* = \frac{2F^2 SL}{\varepsilon_0 \varepsilon_C} \frac{u_p (p_Q + n_Q)^3}{p_Q - n_Q} \frac{r_A}{l_{Bj}} \quad \text{and} \quad p_E \approx p_Q + \frac{p_Q + n_Q}{\mathrm{e}^{I_c^*/I} - 1}$$

where we assumed equal mobilities $u_n = u_p$ to keep the result simple. The critical current I_c^* obtained from integration of the length integral equals that obtained from the first-order approximation of the ion pairing intensity $\mathcal{R}$ given in Eq. (18).

Finally, we calculate the characteristic current I_c given by Eq. (10) by means of the characteristic pairing intensity of Eq. (19). The characteristic current becomes:

$$I_c = \frac{2F^2 SL}{\varepsilon_0 \varepsilon_C} \frac{u_p}{\ln 4 - 1} \frac{(p_Q + n_Q)^3}{p_Q - n_Q} \frac{r_A}{l_{Bj}}$$

Also in this case the critical current I_c^* differs from the characteristic current; however, it is very similar.

Numeric monopolar simulations

The monopolar situation represents the simplest possible ion transport mechanism within the framework of the PNPC equations. Owing to its simplicity, numerical simulations can easily cover a wide range of possible situations. Therefore, we choose the monopolar ion transport mechanism to compare the analytical results of the drift approximation with the numerical results using full Nernst-Planck and Gauss' equations. The details of these equations and their numerical solution are described in the Appendix. The numerical simulations are implemented as Mathematica notebooks as well as C programs. They are available on request via e-mail.

The simulation covers a range of concentrations at the boundaries of $p_Q/50 \le p_B \le 50\, p_Q$; $p_B/p_Q \in \{1/50,\ 1/20,\ 1/10,\ 1/5,\ 1/2,\ 2,\ 5,\ 10,\ 20,\ 50\}$. The internal p_i and external concentrations are defined as $p_i = p_B/\mathrm{e}$ for $p_B < 1$, $p_i = p_B$ for $p_B > 1$, and $p_o = \mathrm{e}\, p_i$. This leads to a reversal potential of 25 mV. For these concentrations at least the following Debye lengths were considered: $L/l_{DH} \in \{1, 3, 5, 7, 10, 20\}$. In some calculations also $L/l_{DH} \in \{2, 4, 14\}$ were included. Current-voltage curves as shown in Fig. 3 have been calculated in the voltage range of $-1.25\ \mathrm{V} \le V \le +1.25\ \mathrm{V}$. This wide voltage range was chosen to see the limiting behavior of those curves beyond the particular range of interest. Figure 3 indicates the general behavior of current-voltage curves that external concentrations above/below the equilibrium concentration corresponds to super-/sublinear current-voltage curves. The sublinearity is rather sharp and disappears at larger voltages, whereas the superlinearity extends over a wide voltage range. This qualitative behavior of the current-voltage curves is found for all concentrations and Debye lengths considered in this study. In the derivation of the drift current-voltage relation [Eq. (9)], we had to make several assumptions about the smallness of some numbers. To get an impression how far the drift approximation applies and what the "$\lll$'s" actually mean, we first present the numerical simulation of some example cases. Later we explore effect of switching off the Gauss equation, i.e., how the full PNPC current-voltage curves differ from those of a purely GHK ion transport mechanism.

Evaluating the drift approximation

To what degree does the drift approximation conform with the simulation of the full PNP equations? A simple and direct test is given in Fig. 4. The drift length L_E and drift voltage V_E defined in Eq. (7) are compared with the actual length L and voltage V. For the shown case of $L/l_{DH} = 5$ the drift length and voltage are in the correct order of magnitude over a wide range of voltages and concentrations. For smaller Debye lengths the curves become flatter, i.e., the relative good agreement is shifted towards larger voltages. For larger Debye lengths the agreement disappears, the drift lengths and voltages become too large: $L_E \ggg L$ and $V_E \ggg V$ (data not shown).

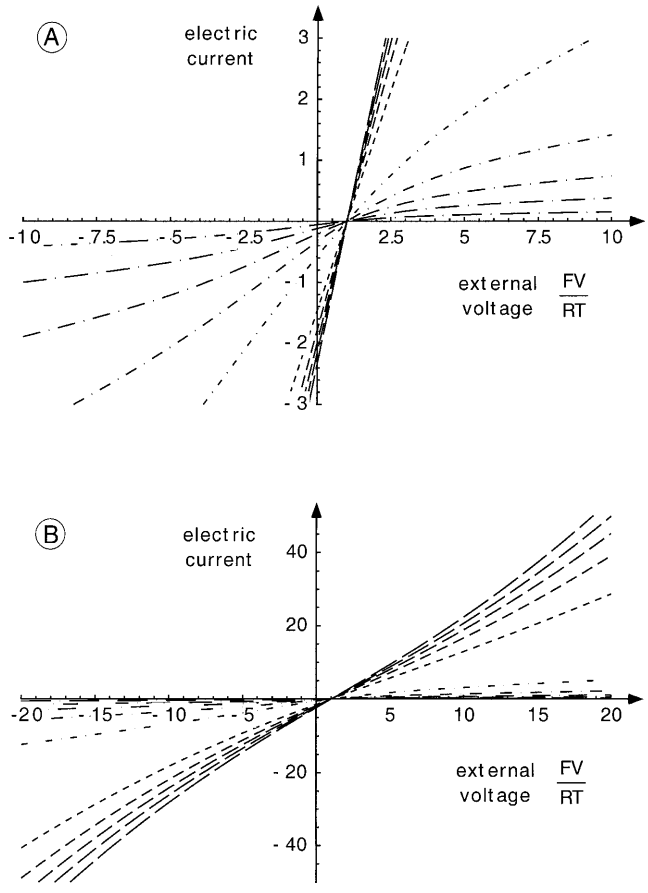

Fig. 3A, B Current-voltage curves for the monopolar ion transport model obtained from numerical solutions of the full PNP equations as a function of the external ion concentrations. The current is given in dimensionless units as defined in the Appendix in Eq. (42). The channel length L divided by the Debye length is $L/l_{DH}=5$. The internal ion concentrations p_i are: $p_i/p_Q \in \{1/(50e), 1/(20e), 1/(10e), 1/(5e), 1/(2e), 2, 5, 10, 20, 50\}$ (see Figs. 1 and 2). The external concentrations are $p_o=p_i e$, which implies a reversal potential of 25 mV. The *dashed curves* indicate external concentrations above the equilibrium concentration p_Q; the dash length corresponds to the concentration. The *dashed-dotted* curves describe current-voltage curves for external concentrations below p_Q. Here, the dash length increases with decreasing concentration. **A** and **B** show the same figure with different scalings for the axis: **A** clearly displays the strong sublinearity for external concentrations below p_Q and **B** the weaker superlinearity for external concentrations above p_Q

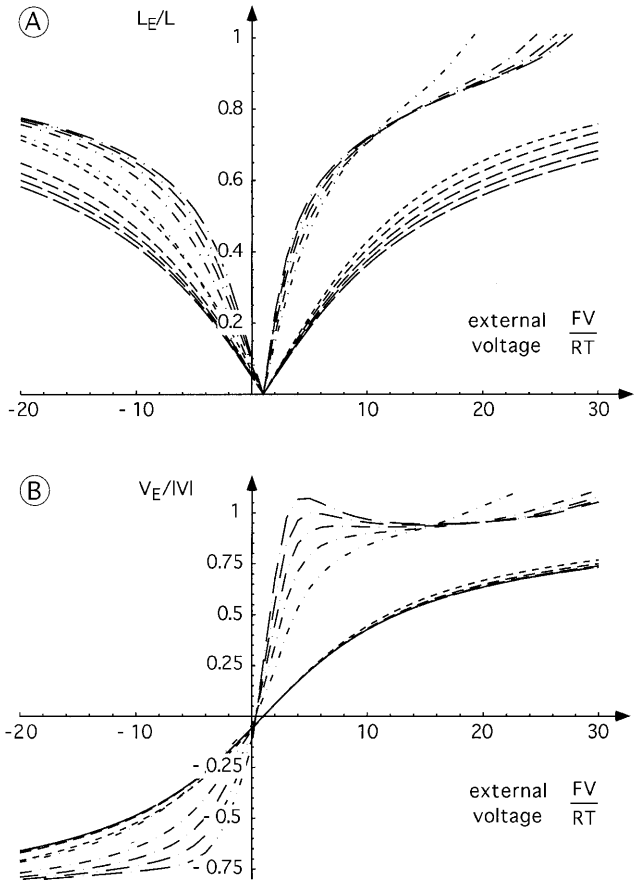

Fig. 4 The approximate analytic drift length (**A**) and voltage (**B**) as defined in Eq. (7) as a function of the external ion concentrations obtained from numerical solutions of the full PNP equations. For the monopolar model it becomes a function of the extreme concentration $p_E=p_Q(1+h_E)$ which is given in the Appendix [Eq. (37)]. For the details of the model parameters, see Fig. 3

Whereas the drift length and voltage can be used to check the applicability of the drift approximation, they are of little practical value. Therefore, we also compared the channel conductance calculated in a previous article (Syganow and von Kitzing 1995). In the Appendix [Eq. (41)] those equations are given in a dimensionless form generalized for asymmetric concentrations. In Table 3, these analytical approximate conductances are compared with the conductivities of the current-voltage curves obtained from numerical solutions of the complete PNP theory for the case of $L/l_{DH}=5$. The PNP conductances are determined in two ways. The fitted conductance $\Sigma^{\pm}_{Fit}$ represents the linear part of the drift current-voltage relation [Eq. (9)] fitted to the PNP current-voltage curve. This fitting procedure agrees closely with the situation of analyzing experimental current-voltage curves. In the second method, the slope of the PNP current-voltage curve at the reversal potential is used to determined the slope conductance Σ_{Slope}. Because of the strong curvature, at small external concentrations ($p_{i/o} \ll p_Q$) the fitted conductances deviate considerably from the respective slope conductances. The fitted values depend critically on the size of the fitting window. The agreement between approximate analytical results and those obtained from PNP current-voltage curves is good despite the approximations necessary to solve the resistance integral (see Appendix). The agreement improves for longer Debye lengths and becomes worse in the opposite case owing to the approximations involved in the resistance integral.

Also for the comparison of the characteristic currents I_c [Eq. (10)], we use the case of $L/l_{DH}=5$. In its dimensionless form, the characteristic current i_c is given in the Appendix [Eq. (42)]. In Table 4 we show the fitted characteristic current $i^{\pm}_{Fit}$ obtained from fitting the current-voltage

Table 3 Numerical and analytical conductances[a]

p_B/p_Q	Σ^+_{Fit}	Σ^-_{Fit}	Σ_{Slope}	Σ_Q	Σ_{Lim}
0.02	−0.03722	0.24037	0.04828	0.04033	0.27675
0.05	−0.15144	0.26915	0.1066	0.09005	0.44191
0.1	−1.0139	0.33464	0.18499	0.1584	0.57607
0.2	1.0255	0.44105	0.30541	0.2663	0.70582
0.5	0.724	0.65132	0.54234	0.4846	0.8612
2.0	1.3865	1.4332	1.4449	1.536	2.3062
5.0	1.7054	1.7262	1.7725	1.9162	2.5175
10.0	1.9089	1.9178	1.9786	2.1654	2.6354
20.0	2.0732	2.0766	2.1455	2.3699	2.7259
50.0	2.2354	2.2362	2.3112	2.5738	2.8127

[a] Approximate analytical and full PNP conductances of the monopolar ion transport model for $L/l_{DH}=5$. $\Sigma^{\pm}_{Fit}$ are the conductivities obtained from fitting the drift current-voltage relation [Eq. (9)] to the current-voltage curves obtained from numerical solutions of the full PNP equations in the range of [−249, 0] mV and [2, 251] mV. Σ_{Slope} is determined from the slope of the PNP current-voltage curve at the reversal potential (see Fig. 3). Σ_Q is the approximate analytical equilibrium conductance [see Appendix, Eq. (41)] with the numerical extremal p_E and actual boundary concentrations p_i and p_o (see Fig. 2), and Σ_{Lim} the equilibrium conductance with the numerical extremal concentration p_E at zero (for $p_B < p_Q$) and infinite (for $p_B > p_Q$) boundary concentrations

Table 4 Numerical and analytical characteristic currents[a]

p_B/p_Q	i^+_{Fit}	i^+_{Drift}	i^+_{Lim}	i^-_{Fit}	i^-_{Drift}	i^-_{Lim}
0.02	0.0543	−0.0155	−0.0027	0.0841	0.1303	0.02
0.05	0.0912	−0.0558	−0.0169	0.5576	0.4861	0.1253
0.1	0.0606	−0.1616	−0.0678	2.2068	1.4939	0.5051
0.2	−0.275	−0.5058	−0.2721	9.3883	5.2772	2.0833
0.5	−3.088	−2.5386	−1.7509	186.08	44.815	16.667
2.0	399.4	175.22	66.667	−132.04	−103.87	−51.751
5.0	224.57	143.47	52.083	−166.13	−131.05	−50.272
10.0	218.6	152.69	50.505	−190.61	−148.86	−50.068
20.0	222.73	164.81	50.125	−209.59	−163.66	−50.017
50.0	229.95	178.87	50.02	−225.59	−178.65	−50.003

[a] Approximate analytical and full PNP characteristic currents of the monopolar ion transport mechanism for $L/l_{DH}=5$ as a function of the boundary concentration p_B. Because the drift limit applies only at larger voltages, the low voltage range $-RT/F < V < +RT/F$ is not covered by this approximation and the current-voltage relations split into positive and negative parts. The dimensionless characteristic currents i_c are given in the Appendix [Eq. (42)]. The index "Fit" indicates the characteristic currents $i^{\pm}_{Fit}$ obtained from fitting the drift current-voltage relation of [Eq. (9)] to the positive and negative branch of the PNP current-voltage curves in the range of [−249, 0] mV and [2, 251] mV (see Fig. 3). $i^{\pm}_{Drift}$ is the drift characteristic current where the extremal concentration p_E from the simulation was used in the calculation. For $i^{\pm}_{Lim}$ we took the equilibrium concentration p_Q (see Fig. 2)

relation of Eq. (9) to the PNP current-voltage curves. This numeric result is compared with the approximate analytical characteristic currents. First we use the numeric extreme p_E and the boundary concentrations p_i and p_o (see Fig. 2) to obtain $i^{\pm}_{Drift}$. To test the replacement of the extreme concentration p_E by the equilibrium concentration p_Q we also considered this case in $i^{\pm}_{Lim}$. One should not expect any exact agreement between PNP and analytical data because the exact PNP values depend on the size of the fitting window. Except for external concentrations $p_{i/o}$ close to the equilibrium concentration, the agreement between $i^{\pm}_{Fit}$ and $i^{\pm}_{Drift}$ is quite good. In contrast, $i^{\pm}_{Lim}$ deviates considerably from the "experimental" value; however, it stays within the order of magnitude. This deviation clearly indicates that it is important to include the deviation of the extreme concentration p_E from the equilibrium concentration p_Q for those parameters considered in this study.

In Fig. 5, monopolar concentration profiles are shown as a function of the external voltage for boundary concentrations $p_{i/o}$ above and below the equilibrium concentration. For the first case, rather large voltage steps have to be taken to make the effect of the increasing external field clearly visible in the concentration profile. The same kind of behavior is seen in the current-voltage curves of Fig. 3, which are only slightly curved and the curvature extends to large external voltages. In contrast, if the boundary concentrations are below the equilibrium concentration p_Q, much smaller changes in the external voltage result in considerable modifications of the concentration profiles. Again this behavior is reflected in the current-voltage curves in Fig. 3; they are strongly curved and become close to linear at larger voltages. With decreasing Debye length the screening increases and the changes due to external voltages become smaller. The changes in the concentration profile explain the kind of deviation from linearity seen in the current-voltage curves. For large external concentra-

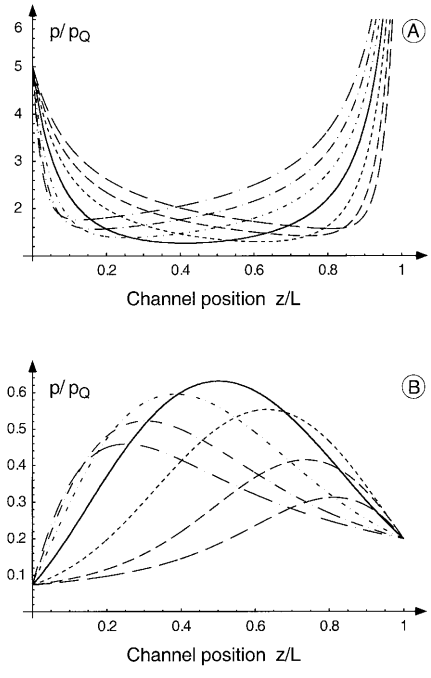

Fig. 5 A, B Concentration profiles at different voltages. For the Debye length of $L/l_{DH}=5$, monopolar concentration profiles are shown, *dot-dashed lines* for negative, *continuous lines* for zero, and *dashed lines* for positive voltages. The dash length corresponds to the voltage. **A** The boundary concentrations are $p_i/p_Q=5$, $p_o/p_Q=5$e, and the voltages $V \in \{-600, -400, -200, 0, 200, 400, 600\}$ mV; **B** $p_Q/p_i=5$e, $p_Q/p_o=5$, and the voltages $V \in \{-300, -200, -100, 0, 100, 200, 300\}$ mV

tions, external ions are driven into the channel with increasing voltage which in turn increases the conductance, resulting in superlinear current-voltage curves. The opposite effect is found for small external concentrations.

Switching from PNP to GHK theory

What is the major influence of Gauss' or Poisson's equation, and why does the PNP conduction mechanism differ so drastically from the one of the GHK theory assuming linear electric fields (Eisenberg 1996)? There exists a long tradition in explaining ion transport by means of GHK theory (Hille 1992). It is still frequently used to evaluate permeabilities from experimental reversal potentials. Therefore, an exploration of the particular differences between the two approaches may help to understand the implications of the more complex PNP theory.

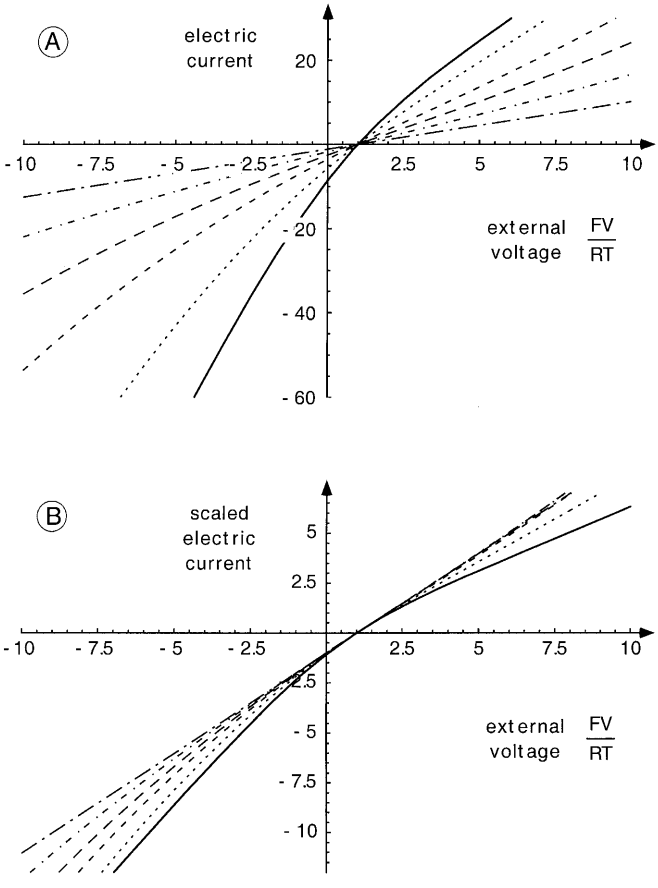

Fig. 6 **A** Current-voltage curves with varying the relative Debye lengths. The quotient of channel length L and the Debye length l_{DH} adopts the values of $L/l_{DH} \in \{0, 1, 2, 3, 5, \text{and } 20\}$ indicated by {a *continuous line*, *dots*, *short dashes*, *long dashes*, *dot short dashes*, and *dot long dashes*}. The boundary concentrations are $p_i/p_Q = 5$ and $p_o/p_Q = 5e$ in all cases. The rectification due to the symmetric external ion concentrations is clearly seen for large Debye lengths (small L/l_{DH}), and it disappears for shorter Debye lengths. **B** The increasing linearity with decreasing Debye length is even more obvious, if the current-voltage curves are divided by the slope conductance at the reversal potential

Figure 6A shows the current-voltage curves of a channel where the external, asymmetric concentrations p_i and p_o are above the equilibrium concentration p_Q inside the channel by $p_i = 5\,p_Q$ and $p_o = 5e\,p_Q$. The quotient between the channel length L and the Debye length l_{DH} ranges from zero (GHK theory) to 20. For a channel with a single permeating ion species the channel is at equilibrium at the reversal potential. Thus, the reversal potential must be independent of the particular interactions between ions and channel protein and among ions. Thus, it is not surprising that the reversal potential is the same for all Debye lengths. With increasing L/l_{DH} the conductance of the channel decreases, as well as the rectification of the current-voltage curves. The disappearance of the rectification becomes even more obvious if each current-voltage curve is divided by its slope conductance at the reversal potential, which is shown in Fig. 6B. At $L/l_{DH} = 20$ the current-voltage curve is practically linear within the voltage range of ±250 mV. Thus, the rectification predicted by GHK theory for asymmetric external solutions is not present in long channels with $L/l_{DH} \gg 1$. Such a lack of rectification is for instance found in the calcium release channel of the sarcoplasmic reticulum of cardiac muscle (Chen et al. 1997). But how can we rationalize this behavior?

Figure 7 shows the concentration profiles at ±250 mV for the Debye lengths used for the current-voltage curves

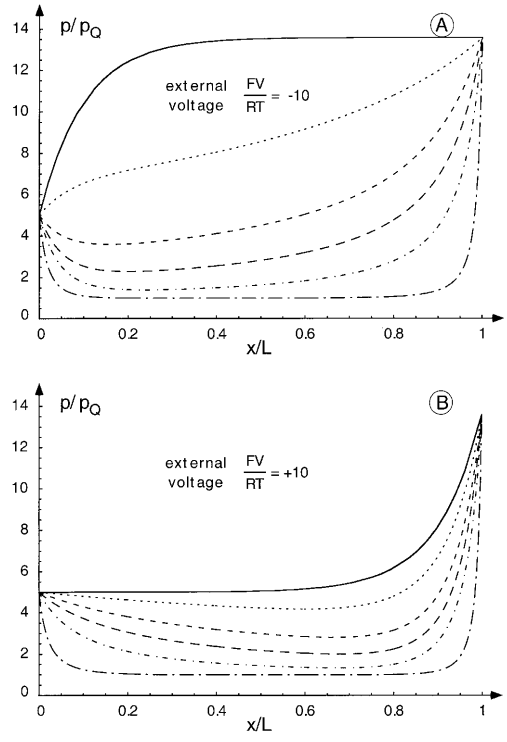

Fig. 7A, B Ion concentration profiles at different Debye lengths. The profiles are shown for **A** $FV/RT = -10$ and **B** $FV/RT = +10$. L/l_{DH} has the same values and the curve pattern the same meaning as in Fig. 6. With decreasing Debye lengths (increasing L/l_{DH}) the ion concentration inside the channel and consequently the channel conductance becomes increasingly independent from the external concentrations and voltage

in Fig. 6. Whereas for the GHK theory the ion concentration along the channel axis is determined by the boundary concentrations and the external voltage, with decreasing Debye lengths (increasing L/l_{DH}) the concentration profile becomes increasingly independent from those parameters. This internal ion concentration is a main determinant for the channel conductance that consequently becomes relatively independent of external influences. Long ion channels define their internal ion concentration, the equilibrium concentration p_Q, independent from the boundary concentrations. The Debye length describes the "flexibility" of the internal ion concentration. If the Debye length is short compared to the channel length, the boundary concentrations p_i and p_o quickly approach the equilibrium concentration p_Q. Similar considerations have been published previously; the L_Ω in Syganow and von Kitzing (1995) indicates the applicability of the drift approximation. For long channels the PNP theory proves the invalidity of the constant field assumption that forms a constituting element of GHK theory. The electric field is constant as long as the space-charge length $l_\rho = \sqrt{RT\varepsilon_0\varepsilon_C/(F|\langle\rho\rangle|)}$ defined previously (Syganow and von Kitzing 1999) is large compared to the channel length L, where $\langle\rho\rangle$ is the average charge density within the channel.

Discussion

In this article we derive explicit current-voltage relations [Eqs. (9)–(11)] for the situation where diffusion-controlled charge transport is dominated by drift due to sufficiently large external voltages. The drift limit of the PNPC equations is based on Gauss' law (2), drift (1), and continuity (3) equations. The external voltage V is approximated by a second-order polynomial in the electric current [Eq. (9)] where the deviation from linear Ohm's law is defined by the characteristic current I_c. The comparison of these approximate analytical results with numerical simulations generally gave a good agreement. It revealed, however, weakness of those relations containing the most extensive approximations. The results of this article explain why many diffusion-controlled ion transport systems show close to linear current-voltage curves, although they generally follow the nonlinear, coupled PNPC equations. Close to linear experimental current voltage-curves can easily be analyzed in terms of a drift current-voltage relation.

Typical examples for diffusion-controlled charge transport systems are biological ion channels. Originally, the drift approximation was developed in the field of semiconductors to explain current-voltage curves of long diodes (Schottky and Spenke 1939; Lampert and Mark 1970; Syganow and Swetchnikow 1981). Here, we present a generalization of those previous contributions to ion transport theories. To discuss practical consequence of the drift approximation, we apply it to biological ion channels. These results differ from those of other particular systems only in the actual values of the system parameters, such as the background charge density, the length of the system, or charge carrier mobilities.

First we present the central properties of the drift current-voltage relation and discuss the approximations involved in its derivation. To show the application of the drift approximation to practical systems, we discuss current-voltage curves of biological ion channels. We particularly demonstrate the importance of pairing in theories of diffusion-controlled ion transport.

What are the approximations involved in the drift current-voltage relation?

To solve the PNPC equations within the drift approximation, we introduce four hierarchical levels of conditions and approximation:

1. At the first level the *drift approximation* [Eqs. (1)–(3)] applies to intermediate and long systems at sufficiently large external voltages. Drift approximation predicts approximate but analytical integral system properties, such as the system length L and the external voltage V given in Eq. (7). By means of these integral properties we derive an explicit drift current-voltage relation [Eq. (9)].
2. At the second level we reduce the applicability of the theory of *long systems* and *low electric currents*. In these limits the extreme specific conductivity σ_E approaches the equilibrium specific conductivity σ_Q (see Fig. 2). Whereas σ_E generally is a function of the electric current, σ_Q is constant. σ_E appears in the characteristic current I_c; its convergence towards σ_Q, therefore, makes I_c current independent.
3. For large or small association rate constants k_A [see Eq. (22)] we introduce the *space-charge* [see Eq. (15)] and the *quasi-neutral* [see Eq. (14)] ion transport mechanisms, respectively, for which either the continuity Eq. (3) or Gauss' law (2) is solved trivially. For each limit we derive algebraic relations between anion and cation concentrations [see Eqs. (27) and (29), respectively].
4. For simple models of ion transport we calculate the respective conditions for the ion transport mechanism, the critical and characteristic currents analytically. We compare the results of the analytical drift approximation for the monopolar space-charge ion transport mechanism with those obtained from numerical solutions of the full PNPC equations.

Drift approximation

At sufficiently large external voltages the drift approximation applies. In this case the contribution of concentration gradients in the Nernst-Planck equation to the current-voltage relation is small. The precise meaning of "large external voltage" depends on the details of the system under consideration. It applies if the Ohmic length $L_\Omega \ll L$ is small [Eqs. (26) and (39) in our previous publication (Syganow

and von Kitzing 1995)]. The value of the Ohmic length L_Ω has the same order of magnitude as the Debye length l_{DH} with the concentration at the boundary. L_Ω was previously derived for the space-charge transport mechanism. An analogous length can be defined for the quasi-neutral case.

Because the drift approximation applies only at large absolute external voltages, the current-voltage relation splits into two separate parts, one for large negative voltages and the other for large positive voltages. Drift ap-proximation predicts a simple current-voltage relation [Eq. (9)] with three free parameters for the positive and negative branches of the current-voltage data: the diffusion voltage V_D (Syganow and von Kitzing 1995) which accounts for the neglected diffusion terms, the Ohmic conductance Σ in the limit of large external voltages, and the characteristic current I_c which accounts for the deviation from Ohm's law owing to pushed-in or drawn-out ions. Positive/negative characteristic currents represent super/sublinear current-voltage curves which indicate the concentration of the ion species carrying the largest electric current to be below/above the external concentration, respectively. Current-voltage curves with large characteristic voltages $|V_c = I_c/\Sigma| \gg RT/F$ generally indicate a drift mechanism for ion permeation, because the two possible alternatives, equilibrium or diffusion mechanism (see introduction), generally have exponential current-voltage relations with characteristic voltages in the order of RT/F (e.g., GHK theory at small voltages $|V| \ll RT/F$ and different external concentrations).

Long system and low current limit

The drift current-voltage relation of Eq. (9) definitely applies to long systems if the internal association length l_A and the internal Debye length l_{DH} are small compared to the system length, $L \gg l_A$ and $L \gg l_{DH}$. The association length l_A, often designated diffusion length, is well known in semiconductor physics (Stöckmann 1961; Lampert and Mark 1970). It is obtained by reformulating the continuity Eq. (3) in dimensionless form:

$$l_A \approx \sqrt{\frac{u_p + u_n}{p_Q + n_Q} \frac{RT}{F k_A}} = l_{DH} \sqrt{\frac{l_{Bj}}{r_A}} \tag{31}$$

The association rate constant k_A was replaced by the expression given in Eq. (24). Thus, the numerical value of the association length has a similar order of magnitude as the Debye length; its particular value is determined by the relation between the Bjerrum length l_{Bj} and the effective association radius r_A [see Eq. (23)]. Within a Debye length l_{DH} the electric field of a permanent or permeant charge is shielded owing to counter ions resulting in a reduced mean electric field around the charge. Within the association length l_A a permeant ion has associated with a permeant counterion.

For long systems the extreme conductivity σ_E approaches the equilibrium conductivity σ_Q in the low current limit [Eq. (17)], as long as the electric current I remains small compared to the critical current ($I_c^*/2 \gg |I|$). Practically, the low current limit implies that the ion concentration inside the channel is not yet dominated by ions pushed into or drawn out of the channel owing to the external voltage, but by the equilibrium concentrations (see Figs. 5 and 7). Our numerical simulations have shown that we get a good agreement between "exact" numerical and approximate analytical results if we replace the equilibrium concentration by the extremal concentration at zero volt. The characteristic current I_c [Eqs. (10) and (19)] is independent of the electric current as long as $I_c/2 \gg I$, and the voltage V in the drift current-voltage relation (9) represents a true second-order polynomial in the current I. From the form of the critical current I_c^* in Eqs. (16) and (18) we concluded earlier that it has the same order as the characteristic current I_c. We confirmed this conclusion in the results section where I_c and I_c^* were calculated analytically for simple models of ion transport. Thus, $|I| \ll |I_c/2|$ is often equivalent to $|I| \ll I_c^*/2$. Consequently, for systems with sufficiently large characteristic currents or equivalently voltages $|V_c| \gg RT/F$ [see Eq. (12)] and not too large external voltages $|V| \ll |V_c|$, the drift approximation generally applies. This particular situation is found for many biological ion channels which are characterized by close to linear current-voltage curves (Dani and Eisenman 1987; Busch 1990; Konno et al. 1991; Villarroel and Sakmann 1992; Kienker et al. 1994; Kuner et al. 1996).

Two limiting ion transport mechanisms

At the third level of approximation we introduce the quasi-neutral [Eq. (14)] and the space-charge ion transport mechanism [Eq. (15)]. They apply for small or large ion association rate constants k_A, respectively. By means of this approximation the anion concentration n can be algebraically expressed as a function of the cation concentration p (or vice versa) by solving Gauss' law (2) or the continuity equation (3) trivially.

The relative "importance" of Gauss' law and the continuity equation is determined by the actual value of the ion association rate constant k_A. On the one hand, large k_A enforce large association and dissociation which requires compensation leading to $\mathcal{R} \approx 0$. Because $\rho \approx 0$ and $\mathcal{R} \approx 0$ in general cannot be fulfilled at the same time except for $p \approx p_Q$ and $n \approx n_Q$, such solutions are characterized by $\rho \neq 0$ and, consequently, designated the space-charge transport mechanism. On the other hand, small association rate constants k_A relax the influence of the continuity equation and emphasize Gauss' law, leading to solutions close to $\rho \approx 0$ with $\mathcal{R} \neq 0$. Consequently, this situation is designated the quasi-neutral ion transport mechanism. In practice, always Gauss' as well as the continuity equations contribute, but the distinction in space-charge and quasi-neutral ion transport mechanisms depicts the dominant behavior of the solutions of the drift approximation in the two limits. The re-

strictions of the two limiting solutions can, for instance, be relaxed by introducing perturbation methods. In the limit of large specific conductivities ($\sigma \gg \sigma_Q$), an analytic solution for the drift approximations was published for arbitrary values of k_A (Parmenter and Ruppel 1959).

Explicit models

At the most specialized level we apply drift approximation to simple detailed models of ion transport. The specific conductivity σ, the charge density ρ, and the recombination intensity $\mathcal{R}$ are expressed as functions of the cation concentration p. The particular models introduced in this article apply to the situation of nearly linear current-voltage curves with a slight superlinearity. This choice keeps the integrals to be solved on an intermediate degree of complexity. The assumption that the channel properties are homogeneous within the cylindrical part of the channel is certainly a strong idealization. Nonner and Eisenberg (Nonner et al. 1998), however, have found in numerical solutions of the PNP equations that even complex channel behavior can be modeled by using homogeneous channel parameters. This finding agrees with our numerical results that even considerable variation in the background charge density does modify the current-voltage curve quantitatively, but not qualitatively (von Kitzing, unpublished results). Thus current-voltage curves often contain not much information about the particular three-dimensional structure of the channel.

Numerical simulations

To obtain an impression of the applicability of the drift approximation we performed numerical simulations of the monopolar ion transport mechanism. The main point to concentrate on, in this case, was keeping the number of adjustable parameters small enough such that we can scan this parameter space exhaustively. A similarly complete set of simulations for the quasi-monopolar case would, on the one hand, add very likely not much to the present study, and, on the other hand, would go beyond the scope of the present work.

Because in the drift current-voltage relation of Eq. (9) the voltage is described as a second-order polynomial in the current, the observables are the conductance Σ and the characteristic current I_c as a function of the external concentrations. In Table 3 the simulated and calculated conductances are compared. They agree within 20% over a wide range of concentrations and Debye length's (Table 3 shows only the case of $L/l_{DH}=5$). Thus, the analytic relations for the channel conductances are rather reliable. For boundary concentrations $p_{i/o}$ not too close to the equilibrium concentration p_Q, the characteristic current I_c using the extreme concentration p_E (see Fig. 2) is not too far from the simulated one as shown in Table 4. If, however, the characteristic current is calculated using the equilibrium concentration p_Q there is a considerable deviation between "experiment" and theory, but the order of magnitude is still obtained. A comparison of current-voltage curves and the concentrations profiles as a function of the external voltage clearly indicates the source of the nonlinearity of the current-voltage curves. For large external concentrations, additional ions are driven into the channel, increasing the channel conductance. The opposite effect takes place at low external concentrations.

Of course, the agreement between drift approximation and simulation is not perfect; this comparison shows that drift approximation gives the correct order of magnitude. The existence of such a kind of approximation is not trivial for the highly nonlinear PNP equations. The drift approximation is certainly important for didactic purposes. It helps to understand why this highly nonlinear PNP theory does produce linear or close to linear current-voltage curves over a wide range of conditions. It also allows for a first estimate of channel parameters from experimental current-voltage curves without having to solve numerically sets of complicated differential equations (A. Villarroel, in preparation). This agreement between theory and "experiment" indicates that diffusion-controlled ion transport often is dominated by drift effects.

The continuity equation in the PNPC theory

In this article, we present a long channel, low current drift approximation based on Gauss' law (2), the drift (1), and continuity (3) equations for the analysis of close to linear current-voltage curves. How relevant are these results for diffusion-controlled ion transport, and how important is the inclusion of pairing? Because ion pairing is neglected in almost all theories describing ion transport through biological ion channels or ion exchange membranes, we now discuss the impact of ion pairing on ion permeation for those systems.

From the fact that the concentration of ion pairs in water and similar media with high dielectric constants ε_C is extremely low (Bockris and Reddy 1970), it is generally concluded that ion pairing can be neglected in these media (Buck 1984). This understanding of the importance of ion pairing is further enhanced because most sophisticated electrolyte theories (McQuarrie 1976) apply to homogeneous systems, where the process of ion pairing for many electrolytes does not play an obvious role. At equilibrium concentrations found in homogeneous equilibrium and steady state systems the continuity equation holds trivially. Ion pairing, however, becomes important particularly for the ion dynamics in heterogeneous non-equilibrium situations. The crucial parameter which determines the influence of ion pairing is not the equilibrium association constant k_A/k_D, but the association rate constant k_A. Consequently, the significance of ion pairing does not depend on the concentration of ion pairs but only on the rate to form them. This implies that the continuity equation mainly changes the dynamics of the system.

Many biophysicists are aware that the constant field approximation may present a real problem in using the GHK

equation, e.g., to estimate relative permeabilities from reversal potentials (Hoppe et al. 1982; Hille 1992). The possible invalidity of the constant currents assumption has been considered only very recently (Syganow and von Kitzing 1999). As shown in Eq. (31), the association length and the Debye length are often of similar orders of magnitude. Table 2 shows a range of typical Bjerrum lengths l_{Bj} and effective association lengths r_A. Consequently, in cases where the constant field assumption is violated, the constant currents assumption is likely to be also violated unless explicitly shown otherwise.

But what kind of ion pairing should we consider within ion channels? Within electrically neutral channels one can expect that the presence of a cation inside the channel increases the likelihood for an anion to enter the channel. But what is the role of pairing in potentially highly charged channels such as the acetylcholine receptor channel? The internal negative charge density in such a channel keeps the concentration of anions extremely low. For instance, the acetylcholine receptor channel contains flexible charged side chains which are likely to follow permeating cations on their way through the channel (von Kitzing 1995). In this case, a contact between a permeant cation and a permanent but flexible anionic side chain is inevitable if the ion passes the channel. Formally, such kind of pairing does not differ much from conventional ion pairing [see also (Syganow and von Kitzing 1999)].

Discriminating experimentally between models

What are the distinguishing characteristics in experimental current-voltage curves indicating one of the different ion transport mechanisms? For instance, GHK theory predicts linear conductance-concentration curves and rectification for asymmetric external solutions. Thus, the GHK conduction mechanism is relatively easy to detect.

Barrier models with a large number of free parameters can model nearly every set of experimental results. But those models often cannot justify the assumptions made to derive them from first principles (Syganow and von Kitzing 1999). Barrier models typically predict nonlinear current-voltage curves, i.e., random changes of parameters of a barrier model with linear current-voltage curves generally result in a model with nonlinear current-voltage curves. Thus, if ion transport is dominated by the presence of barriers and wells, mutations should lead to such a characteristic behavior. At highly asymmetric external concentrations, barrier models generally show rectification (Chen et al. 1997).

In contrast, long ion channels show close to linear current-voltage curves under nearly any circumstances, as long as the ion–ion interaction is dominantly electrostatic. Such a behavior is for instance found in the acetylcholine receptor channel. Virtually every mutation in the acetylcholine receptor channel leads to channels with linear current-voltage curves (Imoto et al. 1988; Konno et al. 1991). This linearity is predicted by PNPC theory even under extremely asymmetric external concentrations (Chen et al. 1997). Also, introducing a nonconstant charge profile only leads to small deviations from linearity (von Kitzing, unpublished results). Thus, close to linear current-voltage curves are very characteristic for long channels, i.e., $L/l_{DH} \gg 1$.

Because the internal concentration in long channels is relatively independent from the external ion concentrations, the conductance–concentration relation should be rather nonlinear in most cases. Saturating behavior may result from weak changes of the internal concentration (Syganow and von Kitzing 1995) as a function of the external concentrations or from the fact that at low external concentrations only a part of the total voltage drops across the channel (Muller and Finkelstein 1972).

It is well known from semiconductor physics (Parmenter and Ruppel 1959; Lampert and Mark 1970) that the quasi-monopolar conduction mechanism generally leads to larger currents than the space-charge conduction mechanism. Direct ion pairing is more difficult to detect. Processes which are based on pairing are generally much slower than purely electrostatic processes. The relaxation of the ion cloud takes the Maxwell time $\tau_M \approx l_{DH}^2/D$, where D is the diffusion constant. A typical value for $\tau_M \approx 1$ ns. The relaxation time for association-dissociation processes yields $\tau_A \approx l_A^2/D$, where the association length is taken from Eq. (31). Because we generally have $l_{DH} \ll l_A$, processes including ion association are indicated by a time constant τ_A large compared to the Maxwell relaxation time τ_M.

Conclusions

Diffusion-controlled ion transport is often described by the non-linear, coupled PNPC equations. Within the drift limit, such systems show close to linear current-voltage curves for which we derive an analytical relation. For long systems at low electric currents this relation further simplifies, and the external voltage becomes a second-order polynomial in the current. The association rate constant for forming ion pairs determines the dynamic behavior of the PNPC equations. The quasi-neutral or space-charge ion transport mechanism correspond to the limits of small or large association rate constants, respectively. Commonly used diffusion-limited reaction rate theories indicate small association rate constants, favoring electroneutrality. For sufficiently simple particular model situations, the coefficients in the current-voltage equation can be calculated analytically. Except for the most extensive approximations, a comparison between the results of solving the full PNPC equation numerically and our approximate analytical relations reveals a generally good agreement between the two.

The dynamics of ion transport inhomogeneous nonequilibrium systems is partly determined by the continuity equations. The influence of the continuity equation depends crucially on the association rate constant and not the equilibrium constant. Thus, even if the concentration of

pairs is negligible, the impact of the continuity equation on the dynamics may become important. The constant currents assumption applies to oppositely charged particles only if the association rate constant is extremely small. According to diffusion-limited reaction rate theories, the value of the association rate constant between oppositely charged particles is generally neither small as required in PNP theory nor large as originally assumed by Schottky (Schottky and Spenke 1939). Therefore, the continuity equation cannot be neglected in ion transport theories unless explicitly shown otherwise.

The rather simple form of the *drift current-voltage relation* explains why so many diffusion-controlled ion transport systems show close to linear current-voltage curves. The drift approximation represents a powerful tool to estimate important parameters of these systems.

Glossary

The numbers in the glossary refer to the equations in which the respective term appears first. The terms are defined in the terminology used in theories of ion transport through biological ion channels. A comparison with terms in other fields is given in Table 1.

z: position inside the ion channel along the channel axis.

j, j_p, j_n: total, cation, and anion electric current densities, respectively (6).

σ, σ_p, σ_n: total, cation, and anion specific electric conductivities of the medium, respectively (1 and 6).

σ_i, σ_o: specific conductivity at the intracellular or extracellular boundary of the ion channel, respectively (7, see Figs. 1 and 2).

σ_Q: specific equilibrium conductivity (8). σ_Q would be found if the length of the channel is extended to infinity. At σ_Q the charge density ρ and the pairing intensity $\mathcal{R}$ vanish.

Σ: drift conductance of the ion channel (9).

V: electric voltage (4) across the channel length L.

V_D: diffusion voltage (9) that accounts for small integral diffusion contributions not included in the pure drift voltage (8). The diffusion voltage V_D should not be mistaken for the reversal potential V_R.

V_c: characteristic voltage (12) that accounts for the deviation of the current-voltage curve from linear Ohm's law in the drift limit.

I: total electric current (4).

I_c: characteristic electric current (9) that accounts for the deviation of the current-voltage curve from linear Ohm's law in the drift limit.

I_c^*: critical current (16) that indicates an upper limit for the electric current for the low current approximation.

$\rho(z)$, $\rho(\sigma)$: total mean electric charge density (2) including permanent and permeant charges. The z dependence is replaced by a σ dependence.

ρ_c: characteristic charge density (19). A weighted average of the charge density inside the channel where the charge density close to the specific conductivity minimum has the largest weight.

$\mathcal{R}(z)$, $\mathcal{R}(\sigma)$: ion pairing intensity (3). The z dependence is replaced by a σ dependence.

$\mathcal{R}_c$: characteristic pairing intensity (19): A weigthed average of the pairing intensity inside the channel where the pairing intensity close to the specific conductivity minimum has the largest weight.

L, S: channel length and cross-section, respectively (4).

u_p, u_n: cation and anion mobility of the permeant ions inside the channel (20).

p, n: cation and anion concentrations of the permeating ions inside the channel (20). An additional index Q indicates the respective equilibrium concentrations which are found when the channel length would be extended to infinity.

k_A, k_D: ion association and dissociation rates, respectively (21).

ε_0: vacuum dielectric constant (2).

ε_X: dielectric constant of medium X, e.g. ε_C is the effective dielectric constant inside the channel (2).

Appendix

Here the details of the numerical solutions of the monopolar ion transport mechanism are presented.

Equations of the monopolar approximation

To get an impression of the overall reliability of the analytic drift approximation, we solved the full PNPC equations numerically. The Nernst-Planck equation, using mobility u instead of the commonly used diffusion constant $D = RT\,u/F$ (Hille 1992), for a single species with concentration c, valency Z, mobility u, and electric current I is given by:

$$-I = S\,RT\,Z\,u\left[\frac{\mathrm{d}c}{\mathrm{d}z} - Z\,\frac{FE}{RT}\,c\right]$$

For the numerical simulation we introduce dimensionless variables:

$$i = \frac{L\,I}{S\,RT\,Z\,u\,c_Q}; \quad x = \frac{z}{L}; \quad \varepsilon = \frac{L\,FE}{RT}$$

$$\text{and} \quad c = c_Q\,[1 + Z\,h(x)] \tag{32}$$

These substitutions lead to the dimensionless Nernst-Planck equation:

$$-i = Z h' - Z \boldsymbol{\mathcal{E}} (1 + Z h) \tag{33}$$

where the prime $'$ indicates the x derivative. In the monopolar approximation, Gauss' equation becomes:

$$\frac{\mathrm{d}E}{\mathrm{d}z} = F Z \frac{c - c_\mathrm{Q}}{\varepsilon_0 \varepsilon_\mathrm{c}}$$

With the dimensionless variables defined in Eq. (32), Gauss' equation simplifies to:

$$\boldsymbol{\mathcal{E}}' = \lambda_\mathrm{DH}^2 h \quad \text{with} \quad \lambda_\mathrm{DH} = L \sqrt{\frac{F^2 Z^2 c_\mathrm{Q}}{RT \varepsilon_0 \varepsilon_\mathrm{c}}} \tag{34}$$

where λ_DH is the quotient of the channel length L and the Debye length l_DH within the channel.

To solve Eqs. (33) and (34) numerically, we differentiate the Nernst-Planck equation (33) and substitute the primed electric field by Gauss' equation (34)

$$0 = h'' - Z \boldsymbol{\mathcal{E}} h' - \lambda_\mathrm{DH}^2 h (1 + Z h) \tag{35}$$

where the conservation of the ions $i' = 0$ is used. In the absence of binding partners, no pairing can occur.

As expected, this Gauss-Nernst-Planck or PNP equation is highly nonlinear. The nonlinearity comes from the product of h and $\boldsymbol{\mathcal{E}}$, because $\boldsymbol{\mathcal{E}}$ is itself a function of h, and from the product of h and $1 + Zh$. Methods to solve the PNP equations are for instance indicated by Buck (1984), Chen (Chen and Eisenberg 1993), or by Nonner (Nonenr and Eisenberg 1998). Here we introduce a different method which can also be extended to ion-pairing (von Kitzing, unpublished results). We introduce a linearization of the PNP Eq. (35) which leads to:

$$0 = h'' - Z \boldsymbol{\mathcal{E}} h' - \lambda_\mathrm{DH}^2 h (1 + Z H) \tag{36}$$

with

$$\boldsymbol{\mathcal{E}}(x) = \boldsymbol{\mathcal{E}}_\mathrm{V} + \lambda_\mathrm{DH}^2 \int_0^x H(y)\, \mathrm{d}y$$

where $\boldsymbol{\mathcal{E}}_\mathrm{V}$ is chosen to yield the external voltage $FV/RT = \int_0^1 \boldsymbol{\mathcal{E}}(x)\, \mathrm{d}x$. For a given nonlinearity of the problem $H(x)$, Eq. (36) represents a linear equation for $h(x)$. By iteratively updating $H(x)$, solutions for the nonlinear Eq. (35) are obtained. This particular form of the linearization of Eq. (35) has the advantage that the consequential discretization leads to a highly sparse matrix which can be solved efficiently by biconjugated gradient methods (Press et al. 1992).

Comparison of numerical and analytical data

To compare the numerical solutions of the PNP equations and the theoretical predictions, we have to bring the theoretical formulas into the non-dimensional form. In the results section we compare the drift length L_E and drift voltage V_E calculated by Eq. (7) with the actual length L and voltage V. If we apply Eq. (32) to the drift Eq. (1) and to the differential length $\mathrm{d}x = \mathrm{d}z/L$ in Eq. (5) we obtain for the drift limit:

$$\boldsymbol{\mathcal{E}} \approx \frac{i}{1 + h} \quad \text{and} \quad dz \approx \frac{i}{\lambda_\mathrm{DH}^2} \frac{\mathrm{d}h}{h(1+h)^2}$$

This leads to the drift length L_E and drift voltage V_E:

$$\frac{L_\mathrm{E}}{L} = \frac{i}{\lambda_\mathrm{DH}^2} \left(\frac{1}{1 + h_\mathrm{B}} - \frac{1}{1 + h_\mathrm{E}} + \ln \left[\frac{h_\mathrm{B}}{h_\mathrm{E}} \frac{1 + h_\mathrm{E}}{1 + h_\mathrm{B}} \right] \right)$$

$$\frac{V_\mathrm{E}}{V} = \frac{i^2}{\lambda_\mathrm{DH}^2} \left(\frac{3 + 2 h_\mathrm{B}}{(1 + h_\mathrm{B})^2} - \frac{3 + 2 h_\mathrm{E}}{(1 + h_\mathrm{E})^2} + \ln \left[\frac{h_\mathrm{B}}{h_\mathrm{E}} \frac{1 + h_\mathrm{E}}{1 + h_\mathrm{B}} \right] \right) \tag{37}$$

For positive or negative voltages, h_i or h_o, respectively, has to be taken instead of h_B. For $L_\mathrm{E} \approx L$ and $V_\mathrm{E} \approx V$ the drift approximation applies. In numerical calculations the extremal h_E is obtained from the simulation.

In a previous article we showed (Syganow and von Kitzing 1995) that the channel conductivity can be calculated from the equilibrium approximation. Here we compare this calculated approximate conductivity with that of the numerical simulation. First we have to introduce the dimensionless equilibrium logarithmic slope κ_Q (phase trajectory):

$$\kappa_\mathrm{Q} = \frac{L}{c(z)} \frac{\mathrm{d}c}{\mathrm{d}z} = \frac{h'}{1 + h} \quad \Rightarrow \quad \mathrm{d}x = \frac{\mathrm{d}h}{\kappa_\mathrm{Q} (1 + h)} \tag{38}$$

Following Eq. (8) given in Syganow and von Kitzing (1995), for the monopolar approximation the logarithmic slope becomes for small electric currents:

$$\kappa_\mathrm{Q}^2 = 2 \lambda_\mathrm{DH}^2 \int_{h_\mathrm{E}}^{h} \frac{g\, \mathrm{d}g}{1 + g} = 2 \lambda_\mathrm{DH}^2 \left[h - h_\mathrm{E} - \ln \frac{1 + h}{1 + h_\mathrm{E}} \right] \tag{39}$$

Integration of $\mathrm{d}x$ in Eq. (38) directly gives a relation for the extremal concentration h_E inside the channel. h_E is positive ($1 + h_\mathrm{Q} > 1$) if the external concentrations are above the equilibrium concentration, and negative ($1 + h_\mathrm{Q} < 1$) in the other case:

$$1 = \int_0^1 \mathrm{d}x = \int_{h_\mathrm{E}}^{h_\mathrm{i}} \frac{\mathrm{d}h}{\kappa_\mathrm{Q} (1 + h)} + \int_{h_\mathrm{E}}^{h_\mathrm{o}} \frac{\mathrm{d}h}{\kappa_\mathrm{Q} (1 + h)}$$

Unfortunately, we know no analytic solution for these integrals. Because κ_Q becomes zero for $h = h_\mathrm{E}$, it contributes most at this point to the integrals. Consequently, we expand κ_Q^2 around h_E and obtain:

$$\kappa_\mathrm{Q}^2 \approx h_\mathrm{E} \frac{h - h_\mathrm{E}}{1 + h_\mathrm{E}}$$

This choice for κ leads to a "channel length":

$$1 \approx \frac{1}{\lambda_\mathrm{DH}} \sqrt{\frac{2}{h_\mathrm{E}}} \times \begin{cases} \arctan w_\mathrm{i} + \arctan w_\mathrm{o} & \text{for } h_\mathrm{i} > 0 \text{ and } h_\mathrm{o} > 0 \\ \operatorname{arctanh} w_\mathrm{i} + \operatorname{arctanh} w_\mathrm{o} & \text{for } h_\mathrm{i} < 0 \text{ and } h_\mathrm{o} < 0 \end{cases} \tag{40}$$

with $w_B = \sqrt{|h_B - h_E|/(1+h_E)}$ and $B \in \{i, o\}$. Numerical tests showed that this approximation works well as long as h_E is not too small, i.e., as long as the Debye length is not too small compared to the channel length: $\lambda_{DH} \gg 1$.

In dimensionless coordinates the resistance of the channel is given by [see Eq. (37) in our previous publication (Syganow and von Kitzing 1995)]:

$$r = \frac{Fuc_Q}{L} R = \frac{Fuc_Q}{L} \int_0^L \frac{dz}{Fuc(z)} = \int_{h_E}^{h_B} \frac{dh}{\kappa(1+h)^2}$$

Here, we have the same difficulty as in the case of the length calculation, the logarithm in the logarithmic slope prevents an analytical solution of the integral. Therefore, we use the same approximation as in the case of the channel length. To reduce the effect at small h_E, divide this result by the approximate "channel length" given in Eq. (40). Taking the reverse of the resistance we obtain the unit-free conductivity s of the channel:

$$s \approx 2 \frac{\text{at } w_i + \text{at } w_o}{\frac{w_i}{1+h_i} + \frac{w_o}{1+h_o} + \frac{\text{at } w_i + \text{at } w_o}{1+h_E}}$$

$$\text{at} = \begin{cases} \arctan & \text{for } h_i > 0 \text{ and } h_o > 0 \\ \operatorname{arctanh} & \text{for } h_i < 0 \text{ and } h_o < 0 \end{cases} \qquad (41)$$

In the monopolar drift approximation the deviation from linear Ohm's law is given by the characteristic charge density ρ_c defined in Eq. (19). In unit-free notation we obtain:

$$\frac{Fc_Q}{\rho_C} = \frac{1}{h_C} = Fc_Q \sigma_E \int_{\sigma_E}^{\sigma_B} \frac{\sigma - \sigma_E}{\rho \sigma^3} dh$$

$$= (1+h_E) \int_{h_E}^{h_B} \frac{h - h_E}{h(1+h)^3} dh$$

and the dimensionless characteristic current i_c becomes:

$$i_c = \frac{L I_C}{S RT u c_Q} = \lambda_{DH}^2 (1+h_E) h_C$$

$$= 2\lambda_{DH}^2 \Bigg/ \left[\frac{(h_B - h_E)(2 + h_B + 3h_E + 2h_B h_E)}{(1+h_B)^2 (1+h_E)} + 2h_E \ln\left(\frac{h_E}{h_B} \frac{1+h_B}{1+h_E} \right) \right] \qquad (42)$$

Iterative solution of the PNP equation

For using Eq. (36) an initial estimate for the nonlinearity $H(x)$ is needed. The trivial choice is the constant field assumption, i.e., to set $H_0 = 0$. Then the electric field equals FV/RTL. Sometimes one can also use the result of previous calculations. During the evaluation of current-voltage curves, the final result of h at the previous voltage may serve as the initial choice for H_0 at the new voltage.

A typical case of fixed point methods would be to calculate h_0 as a linear solution of Eq. (36) with H_0 as the first nonlinearity. In the next step, the nonlinearity is updated using the simple relation: $H_{k+1} = h_k$. This procedure can be repeated until convergence is obtained. Unfortunately, the convergence of this procedure is often slow; the procedure may even diverge. Therefore, we modified the simple fixed point algorithm by introducing a calculated relaxation parameter α.

The procedure to solve the nonlinear PNP equation is given in form of a pseudo code. The concentration c and the respective h-function is discretized along the x-axis into n grid points. Thus, $\vec{h}$, $\vec{H}$ and $\vec{\varepsilon}$ are vectors. The dot $\cdot$ represents the Euclidian scalar product. The square implicitly implies the scalar product. Because in the nonlinear problem $\vec{H}$ equals $\vec{h}$, the difference between the two is used as the convergence criteria. The new nonlinearity $\vec{H}_{k+1}$ is calculated from two previous solutions $\vec{h}_k$ and $\vec{h}_{k-1}$: $\vec{H}_{k+1} := \alpha \vec{h}_k + (1-\alpha) \vec{h}_{k-1}$. α_k is chosen to minimize the expected error, where a linear relationship between adjacent $\vec{h}$'s and $\vec{H}$'s is assumed:

$$\min_\alpha \left[(\alpha_k \vec{h}_k + (1-\alpha_k)\vec{h}_{k-1}) - (\alpha_k \vec{H}_k + (1-\alpha_k)\vec{H}_{k-1}) \right]^2$$

This condition directly leads to the linear estimate of α_k:

$$\alpha_k = \frac{\vec{\delta}_{k-1} \cdot \vec{\Delta}_k}{\vec{\Delta}_k \cdot \vec{\Delta}_k}, \quad \text{with} \quad \vec{\delta}_k = \vec{h}_k - \vec{H}_k; \quad \text{and} \quad \vec{\Delta}_k = \vec{\delta}_k - \vec{\delta}_{k-1}$$

Using this relaxation coefficient α_k to update the nonlinearity $\vec{H}_{k+1}$ stabilizes the iteration considerably. For many parameter choices it ensures a fast convergence:

procedure Solve($\vec{H}_0$)
$\vec{H}_0$ is provided by the user.
$\vec{\varepsilon}_0 := \vec{f}(\vec{H}_0)$ is calculated from $\vec{H}_0$.
$\vec{h}_0 := \vec{g}(\vec{H}_0, \vec{\varepsilon}_0)$ results from solving Eq. (36)
$\vec{\delta}_0 := \vec{h}_0 - \vec{H}_0$;
$k := 1$; $\vec{H}_k := \vec{h}_0$; $\vec{\varepsilon}_k := \vec{f}(\vec{H}_k)$; $\vec{h}_k := \vec{g}(\vec{H}_k, \vec{\varepsilon}_k)$
and $\vec{\delta}_k := \vec{h}_k - \vec{H}_k$;
do
$\vec{\Delta}_k := \vec{\delta}_k - \vec{\delta}_{k-1}$; $\alpha_k := -(\vec{\delta}_{k-1} \cdot \vec{\Delta}_k)/\vec{\Delta}_k^2$;
$\vec{H}_{k+1} := \alpha_k \vec{h}_k + (1-\alpha_k)\vec{h}_{k-1}$;
$k := k+1$; $\vec{\varepsilon}_k := \vec{f}(\vec{H}_k)$ and $\vec{h}_k := \vec{g}(\vec{H}_k, \vec{\varepsilon}_k)$;
$\{\vec{H}_k, \vec{h}_k\} := \text{LineSearch}(\vec{H}_k, \vec{h}_k, \vec{H}_{k-1}, \vec{h}_{k-1})$;
$\vec{\delta}_k := \vec{h}_k - \vec{H}_k$;
while $\varepsilon < \vec{\delta}_k^2$ **or** $k < k_{max}$
return $(k, \sqrt{\vec{\delta}_k^2/n}, \vec{h}_k)$
end Solve.

The line search routine is included in this iterative procedure for cases where the linear interpolation fails to provide good new nonlinearities $\vec{H}_{k+1}$. This happens for small Debye length's ($\lambda_{DH} \gg 1$) and large concentrations at the

channel boundaries (c_L, $c_R \gg c_Q$). For those cases the line search algorithm improves the stability of the iterative solution:

procedure LineSearch($\vec{H}_1, \vec{h}_1, \vec{H}_0, \vec{h}_0$)
$\vec{\delta}_0 := \vec{h}_0 - \vec{H}_0$; $l := 1$;
begin loop
$\vec{\delta}_l := \vec{h}_l - \vec{H}_l$; $\vec{\Delta}_l := \vec{\delta}_l - \vec{\delta}_0$;
$\alpha_l := -(\delta_0 \cdot \Delta_l)/\Delta_l^2$;
if $\delta_l^2 < \delta_0^2$ **or** $l \geq l_{\max}$ **then return** $\{\vec{H}_l, \vec{h}_l\}$;
$\vec{H}_{l+1} := \alpha_l \vec{H}_l + (1-\alpha_l)\vec{H}_0$;
$l := l+1$; $\vec{\varepsilon}_l := \vec{f}(\vec{H}_l)$; $\vec{h}_l := \vec{g}(\vec{H}_l, \vec{\varepsilon}_l)$
end loop
end LineSearch.

The major difference between the general iteration and the line search procedure is that in the former the new nonlinearity is updated using $\vec{h}_k$ and $\vec{h}_{k-1}$ and in the latter $\vec{H}_l$ and $\vec{H}_0$ are used.

Acknowledgements The authors would like to thank Drs. Bergling, Burnashev, Villarroel, and Wollmuth for critical reading of the article, Profs. Eisenberg and Karlin for helpful suggestions on an earlier version of the manuscript, and Prof. Sakmann for encouraging and commenting on this work. The numerical solutions of the PNPC equations were obtained using the Mathematica (Wolfram 1991) program package.

References

Barcilon V, Chen DP, Eisenberg RS, Jerome JW (1997) Qualitative properties of steady-state Poisson-Nernst-Planck systems-perturbation and simulation study. SIAM J Appl Math 57: 631–648

Bek S, Jakobsson E (1994) Brownian dynamics study of a multiply-occupied cation channel: application to understanding permeation in potassium channels. Biophys J 66: 1028–1038

Blum L (1980) Primitive electrolytes in the mean spherical approximation. In: Eyring H, Henderson D (eds) Theoretical chemistry: advances and perspectives, vol 5. Academic Press, New York, pp 1–66

Bockris JOM, Reddy AKN (1970) Modern electrochemistry. Plenum Press, New York

Buck RP (1984) Kinetics of bulk and interfacial ionic motion: microscopic bases and limits for the Nernst-Planck equation applied to membrane systems. J Membr Sci 17: 1–62

Busch C (1990) Struktur-Funktions-Untersuchungen am nikotinischen Acetylcholin-Rezeptor. PhD thesis, Ruhr-Universität, Bochum

Calef DF, Deutch JM (1983) Diffusion-controlled reactions. Ann Rev Phys Chem 34: 493–524

Chen D, Xu L, Tripathy A, Meissner G, Eisenberg B (1997) Permeation through the calcium-release channel of cardiac-muscle. Biophys J 73: 1337–1354

Chen DP, Eisenberg RS (1993) Charges, currents, and potentials in ionic channels of one conformation. Biophys J 64: 1405–1421

Chen DP, Barcilon V, Eisenberg RS (1992) Constant fields and constant gradients in open ionic channels. Biophys J 61: 1372–1393

Chung SH, Hoyles M, Allen T, Kuyucak S (1998) Study of ionic currents across a model membrane channel using brownian dynamics. Biophys J 75: 793–809

Cooper K, Jakobsson E, Wolynes P (1985) The theory of ion transport through membrane channels. Prog Biophys Mol Biol 46: 51–96

Dani JA, Eisenman G (1987) Monovalent and divalent cation permeation in acetylcholine receptor channels. Ion transport related to structure. J Gen Physiol 89: 959–983

Ebeling W, Scherwinski K (1983) On the estimation of theoretical individual activity coefficients of electrolytes. Z Phys Chem (Leipzig) 264: 1–14

Eisenberg RS (1996) Computing the field in proteins and channels. J Membr Biol 150: 1–25

Ermak DL, McCammon JA (1978) Brownian dynamic with hydrodynamic interactions. J Chem Phys 69: 1352–1360

Eyring H, Lumry R, Woodbury JW (1949) Some applications of modern rate theory to physiological systems. Rec Chem Prog 10: 100–114

Goldman DE (1943) Potential, impedance, and rectification in membranes. J Gen Physiol 27: 37–60

Hille B (1992) Ionic channels of exitable membranes, 2nd edn. Sinauer, Sunderland, Mass

Hodgkin AL, Katz B (1949) The effect of sodium ions on the electrical activity of the giant axon of the squid. J Physiol (Lond) 108: 37–77

Hoppe W, Lohmann W, Markl H, Ziegler H (1982) Biophysics. Springer, Berlin Heidelberg New York, pp 860–907

Imoto K, Busch C, Sakmann B, Mishina M, Konno T, Nakai J, Bujo H, Mori Y, Fukuda K, Numa S (1988) Rings of negatively charged amino acids determine the acetylcholine receptor channel conductance. Nature 335: 645–648

Jackson JD (1962) Classical electrodynamics. Wiley, New York

Kienker P, Tomaselli G, Jurman M, Yellen G (1994) Conductance mutations of the nicotinic acetylcholine receptor do not act by a simple electrostatic mechanism. Biophys J 66: 325–334

Kitzing E von (1995) Structure modeling of the acetylcholine receptor channel and related ligand gated channels. In: Pullman A, Jortner J, Pullman B (eds) Modelling of biomolecular structures and mechanisms, Vol 27. Kluwer, Dordrecht, pp 39–57

Konno T, Busch C, Kitzing E von, Imoto K, Wang F, Nakai J, Mishina M, Numa S, Sakmann B (1991) Rings of anionic amino acids as structural determinants of ion selectivity in the acetylcholine receptor channel. Proc R Soc Lond B 244: 69–79

Kramers HA (1940) Brownian motion in a field of force and the diffusion model of chemical reactions. Physica 7: 284–304

Kuner T, Wollmuth LP, Karlin A, Seeburg PH, Sakmann B (1996) Structure of the Nmda receptor channel M2 segment inferred from the accessibility of substituted cysteines. Neuron 17: 343–352

Laidler KJ, King MC (1983) The development of transition-state theory. J Phys Chem 87: 2657–2664

Lampert MA, Mark P (1970) Current injection in solids. Academic Press, New York

Levitt DG (1991a) General continuum theory for multi-ion channel, (1) theory. Biophys J 59: 271–277

Levitt DG (1991b) General continuum theory for multi-ion channel, (2) application to acetylcholine channel. Biophys J 59: 278–288

MacGillivray AD (1967) Nernst-Planck equations and the electroneutrality and Donnan equilibrium assumptions. J Chem Phys 48: 2903–2907

MacGillivray AD, Hare D (1969) Applicability of Goldman's constant field assumption to biological systems. J Theor Biol 25: 113–126

Mafé S, Pellicer J, Aguilella VM (1986) Ionic transport and space charge density in electrolytic solutions as described by Nernst-Planck and Poisson equations. J Phys Chem 90: 6045–6050

Mafé S, Pellicer J, Aguilella VM, Garrido J (1987) A study of the failure of the electroneutrality assumption in the vicinity of the inner membrane boundaries. J Non-Equilib Thermodyn 12: 161–168

McQuarrie DA (1976) Statistical mechanics. Harper & Row, New York

Muller RU, Finkelstein A (1972) The effect of surface charge on the voltage-dependent conductance induced in thin lipid membranes by monazomycin. J Gen Physiol 60: 285–306

Nonner W, Eisenberg B (1998) Ion permeation and glutamate residues linked by Poisson-Nernst-Planck theory in L-type calcium channels. Biophys J 75: 1287–1305

Nonner W, Chen DP, Eisenberg B (1998) Anomalous mole fraction effect, electrostatics, and binding in ionic channels. Biophys J 74: 2327–2334

Oelkers EH, Helgeson HC (1993) Multiple ion association in supercritical aqueous solutions of single electrolytes. Science 261: 888–891

Offner FF (1971) Nernst-Planck diffusion equation: numerical solution of the boundary value problem. J Theor Biol 31: 215–227

Park JH, Jerome JW (1997) Qualitative properties of steady-state Poisson-Nernst-Planck systems – mathematical study. SIAM J Appl Math 57: 609–630

Parmenter RM, Ruppel MJ (1959) Two carrier space-charge limited currents in a trap-free insulator. J Appl Phys 30: 1548–1558

Pekar SI (1941) Theory of metal-semiconductor contacts and the potential close to the electrode (in Russian). Istvest Akad Nauk SSSR Phys Ser 5: 422–433

Pekar SI (1950) Concerning the theory of electron recombination in semiconductors. Zh Eksp Teor Fiz 20: 267–270

Peskoff A, Bers DM (1988) Electrodiffusion of ions approaching the mouth of a conducting membrane channel. Biophys J 53: 863–875

Planck M (1890) Über die Erzeugung von Elektrizität und Wärme in Elektrolyten. Ann Phys Chem NF 39: 161–186

Press WH, Teukolsky SA, Vetterling WT, Fannery BP (1992) Numerical recipes in C, 2nd edn. Cambridge University Press, Cambridge

Rose A (1978) Concepts in photoconductivity and allied problems. Krieger, Huntington

Rubinstein I (1990) Electro-diffusion of ions. SIAM, Philadelphia

Schottky W, Spenke E (1939) Zur quantitativen Durchführung der Raumladungs- und Randschichttheorie der Kristallgleichrichter. Mitt Zentralabt Zentrallab Fernmeldetech Wernerwerk Siemens Halske 18: 225–291

Smoluchowski MV (1917) Versuch einer mathematischen Theorie der Koagulation kolloider Lösungen. Z Phys Chem (Leipzig) 92: 129–147

Soumpasis DM (1984) Statistical mechanics of the B–Z transition of DNA: contribution of diffuse ionic interactions. Proc Natl Acad Sci USA 81: 5116–5120

Sridharan S, McCammon JA, Hubbard JB (1989) Diffusion-controlled reactions of ions in fluctuating ionic atmospheres. J Chem Phys 90: 237–240

Stöckmann F (1961) Über Strom-Spannungskennlinien ohmscher Kontakte bei Halbleitern und Isolatoren. Vieweg, Braunschweig

Syganow AN, Swetchnikow SW (1981) Injection contact effects in semiconductors (in Russian). Naukow Dumka, Kiew

Syganow AN, Kitzing E von (1995) The integral weak diffusion and diffusion approximations applied to ion transport through biological ion channels. J Phys Chem 99: 12030–12040

Syganow AN, Kitzing E von (1999) (In)validity of the constant field and constant currents assumptions in theories of ion transport. Biophys J 76: 768–781

Sze SM (1981) Physics of semiconductors devices, 2nd edn. Wiley, New York

Triolo R, Grigeria JR, Blum L (1976) Simple electrolytes in the mean spherical approximation. J Chem Phys 80: 1858–1861

Villarroel A, Sakmann B (1992) Threonine in the selectivity filter of the acetylcholine receptor channel. Biophys J 62: 196–208

Weiss GH (1986) Overview of theoretical models for reaction rates. J Stat Phys 42: 3–36

Wolfram S (1991) Mathematica – a system for doing mathematics by computer, 2nd edn. Addison-Wesley, Redwood City